



OPEN ACCESS

EDITED BY

Wagdy Mohamed Eldehna,
Kafrelsheikh University, Egypt

REVIEWED BY

Ahmed Sabt,
National Research Centre, Egypt
Moataz Ahmed Shaldam,
Kafrelsheikh University, Egypt
Mahmoud Rashed,
University of Bonn, Germany

*CORRESPONDENCE

Assem Barakat,
✉ ambarakat@ksu.edu.sa

RECEIVED 19 December 2023

ACCEPTED 14 February 2024

PUBLISHED 08 April 2024

CITATION

Barakat A, Alshahrani S, Al-Majid AM, Alamary AS, Haukka M, Abu-Serie MM, Dömling A, Domingo LR and Elshaier YAMM (2024), Activation of p53 signaling and regression of breast and prostate carcinoma cells by spirooxindole-benzimidazole small molecules.
Front. Pharmacol. 15:1358089.
doi: 10.3389/fphar.2024.1358089

COPYRIGHT

© 2024 Barakat, Alshahrani, Al-Majid, Alamary, Haukka, Abu-Serie, Dömling, Domingo and Elshaier. This is an open-access article distributed under the terms of the [Creative Commons Attribution License \(CC BY\)](https://creativecommons.org/licenses/by/4.0/). The use, distribution or reproduction in other forums is permitted, provided the original author(s) and the copyright owner(s) are credited and that the original publication in this journal is cited, in accordance with accepted academic practice. No use, distribution or reproduction is permitted which does not comply with these terms.

Activation of p53 signaling and regression of breast and prostate carcinoma cells by spirooxindole-benzimidazole small molecules

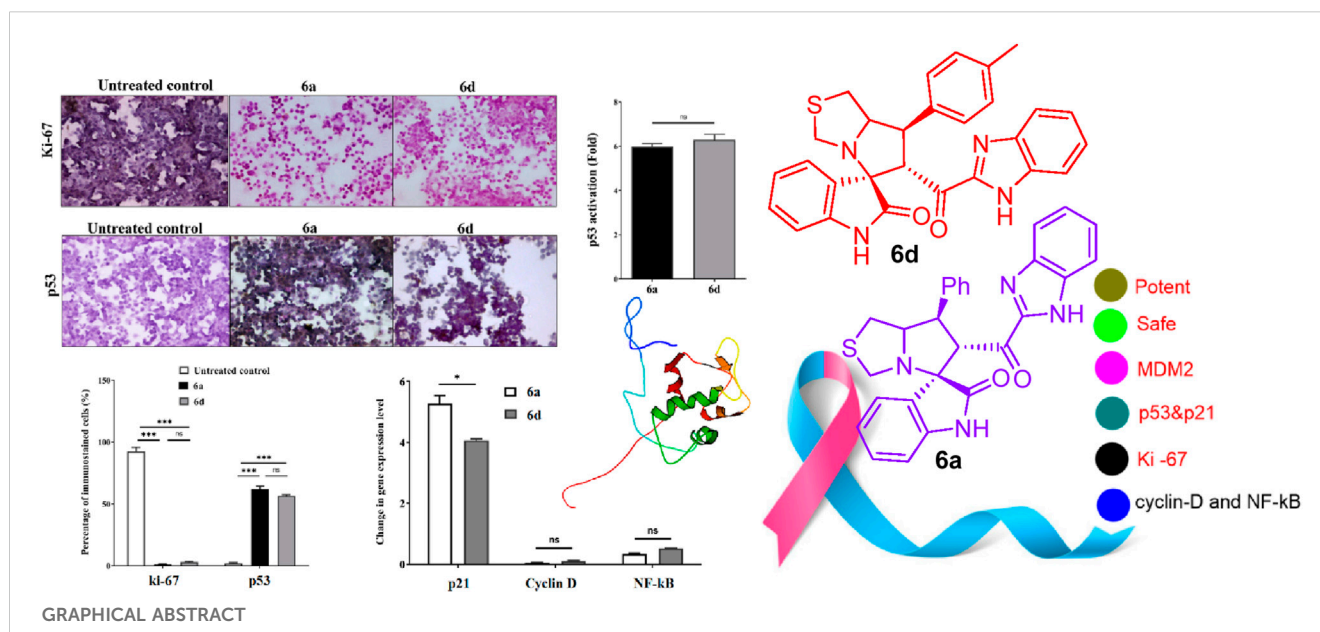
Assem Barakat^{1*}, Saeed Alshahrani¹,
Abdullah Mohammed Al-Majid¹, Abdullah Saleh Alamary¹,
Matti Haukka², Marwa M. Abu-Serie³, Alexander Dömling⁴,
Luis R. Domingo⁵ and Yaseen A. M. M. Elshaier⁶

¹Department of Chemistry, College of Science, King Saud University, Riyadh, Saudi Arabia, ²Department of Chemistry, University of Jyväskylä, Jyväskylä, Finland, ³Medical Biotechnology Department, Genetic Engineering and Biotechnology Research Institute, City of Scientific Research and Technological Applications (SRTA City), Alexandria, Egypt, ⁴Institute of Molecular and Translational Medicine, Faculty of Medicine and Dentistry, and Czech Advanced Technology and Research Institute, Palack University, Olomouc, Czechia, ⁵Department of Organic Chemistry, University of Valencia, Valencia, Spain, ⁶Department of Organic and Medicinal Chemistry, Faculty of Pharmacy, University of Sadat City, Menoufiya, Egypt

This study discusses the synthesis and use of a new library of spirooxindole-benzimidazole compounds as inhibitors of the signal transducer and activator of p53, a protein involved in regulating cell growth and cancer prevention. The text includes the scientific details of the [3 + 2] cycloaddition (32CA) reaction between azomethine ylide **7a** and ethylene **3a** within the framework of Molecular Electron Density Theory. The mechanism of the 32CA reaction proceeds through a *two-stage one-step* process, with emphasis on the highly asynchronous transition state structure. The anti-cancer properties of the synthesized compounds, particularly **6a** and **6d**, were evaluated. The inhibitory effects of these compounds on the growth of tumor cells (MDA-MB 231 and PC-3) were quantified using IC₅₀ values. This study highlights activation of the p53 pathway by compounds **6a** and **6d**, leading to upregulation of p53 expression and downregulation of cyclin D and NF-κB in treated cells. Additionally, we explored the binding affinity of spirooxindole analogs, particularly compound **6d**, to MDM2, a protein involved in regulation of p53. The binding mode and position of compound **6d** were compared with those of a co-crystallized standard ligand, suggesting its potential as a lead compound for further preclinical research.

KEYWORDS

spirooxindole, benzimidazole, MEDT, p53, MDM2 inhibitors, NF-κB, CDK (cyclin-dependent kinase)



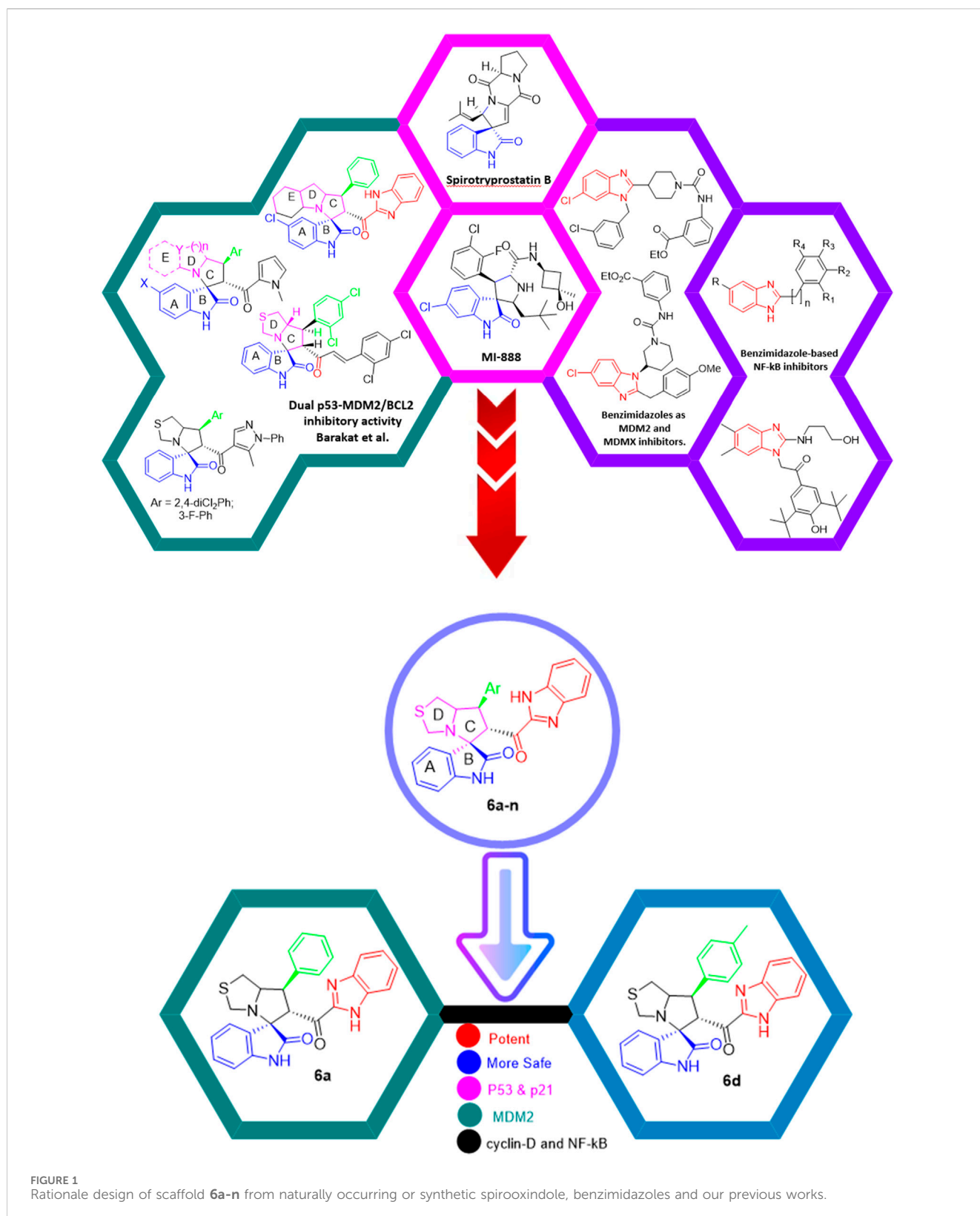
1 Introduction

Many diseases have become more common as a result of natural, industrial, and economic issues. Cancer is the second-leading cause of death worldwide, affecting health in all societies. Unfortunately, it is a tissue-level disease, which presents a major challenge in specific diagnosis and treatment efficacy. Prostate, lung, and colorectal cancers are the most common cancers in men worldwide, accounting for 46% of all newly diagnosed cancers in 2021. Breast cancer is the most common cancer in women worldwide, representing 30% of new cases diagnosed in 2021 (Siegel et al., 2021). Cancer is caused by successive mutations in genes that alter cellular functions proliferation and apoptosis (Chaudhry et al., 2022).

p53 is one of the most-studied tumor-suppressor proteins (Kandoth et al., 2013). Mutations in this protein are found in 60% of human cancers. Changing the DNA binding domain inhibits p53 activity as a transcription factor (Janjua, 2004; Estrada-Ortiz et al., 2016); there is evidence to suggest that restoration or reactivation of p53 function has significant therapeutic benefits (Di Agostino et al., 2006; Demma et al., 2010). The p53 pathway is inactivated in the remaining tumors either by downregulation of p53 cooperators such as ARF or upregulation of p53 inhibitors such as mouse double-minute proteins (MDM2 and MDMX) or downregulation of p53 cooperators such as ARF (Hsu and Ip, 2011). Mutations in p53 and upregulation of MDM2 do not typically occur in the same tumor, indicating that MDM2 overexpression is an effective pathway for inactivating p53 function in tumorigenesis. MDM2 inhibits the N-terminal transactivation domain (TAD) of p53 and promotes p53 degradation via the ubiquitin–proteasome system (E3 ligase activity). Substantial data have confirmed that MDM2 is the central node of the p53 pathway. Genetic and biochemical researchers have mapped MDM2–p53 interaction sites to the 106–amino acid-long N terminal domain of MDM2 and the N-terminus of the transactivation domain of p53. Interaction

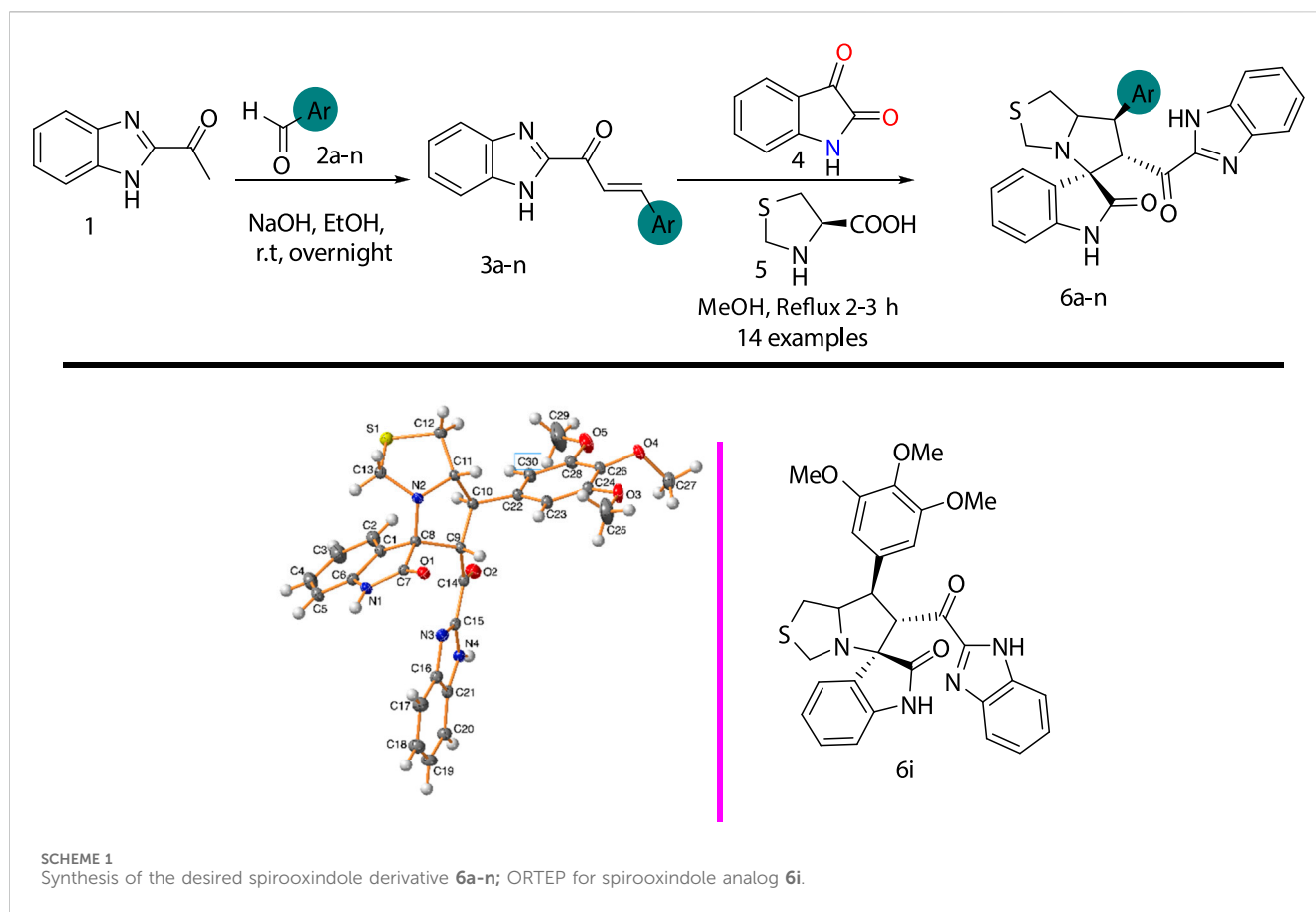
between p53 and MDM2 involves four key hydrophobic residues (Phe 19, Leu 22, Trp 23, Leu 26) in a short amphipathic helix formed by p53 and a small but deep hydrophobic pocket in MDM2. Atomic-level understanding of the MDM2–p53 interaction through x-ray crystallography provides a solid foundation for structure-based design of nonpeptidic, small-molecule antagonists of this interaction (Chen et al., 1993; Kussie et al., 1996). Herein, we set our design rationale to tailor new MDM2 inhibitors endowed with nuclear factor (NF)-κB inhibitory potential to maximize p53 induction capacity (such as enhancing the expression of p21-arrested cell cycle). Previous studies have illustrated that p53 acts as a unique regulator for suppressing NF-κB and aids in preventing its binding to promoter DNA binding sites (Murphy et al., 2011) NF-κB may become overactive in cancer cells because p53 activity is lost (Murphy et al., 2011). NF-κB is an essential transcription factor for expressing several key genes for tumor progression, angiogenesis, and metastasis (Xia et al., 2014; Pires et al., 2017). Thus, it is critical to evaluate the impact of these spirooxindoles on both key transcription factors (p53 and NF-κB).

Several examples based on spirooxindoles (Islam et al., 2023) and benzimidazole core structures have been identified for binding with the MDM2 receptor and activating p53 (Figure 1) (Vassilev, 2007; Li et al., 2008; Riedinger and McDonnell, 2009; Millard et al., 2011; Tovar et al., 2013; Zhao et al., 2013; Zhang et al., 2014; Gollner et al., 2016b; Barakat et al., 2019; Islam et al., 2019; Beloglazkina et al., 2020; Aziz et al., 2021; Lotfy et al., 2021; Barakat et al., 2022). Barakat et al. designed a new lead compound based on the core structure of spirooxindole clubbed with a benzimidazole moiety that has been shown to be highly effective against cancer cells targeted as inhibitors of protein–protein interaction between MDM2–p53 genes. This compound also exhibited a potential anti-metastatic effect (Islam et al., 2019; Aziz et al., 2021; Lotfy et al., 2021; Barakat et al., 2022). With this finding and the high potentiality of the benzimidazole nucleus toward cancer treatment-targeted NF-κB (Okolotowicz et al., 2010; Poltz and Naumann, 2012; Boggu et al., 2016; Jonak et al., 2016; Boggu et al., 2017; Dunphy et al.,



2018; Błaszczak-Świątkiewicz, 2019), we were encouraged to increase the libraries of these analogs and assess them against different cancer cells. Based on the abovementioned data, the rationale design of this work was conceptualized by merging some key features from naturally occurring spirooxindoles with

anticancer activities; reported Benzimidazole-based NF-κB inhibitors; our previous works with dual p53-MDM2/BCL2 (A, B,C,D,E system); and previous spirooxindoles-imidazole hybrid with A, B,C,D,E system. The designed compounds contain spirooxindoles-imidazole with A, B,C,D system.



2 Results and discussion

2.1 Chemistry

To increase the library of spirooxindole scaffolds as lead compounds for development of new drugs for cancer treatment targeting MDM2 inhibitors (Alshahrani et al., 2023), new spirooxindole derivatives (**6a-n**) were synthesized by the reaction of chalcones **3a-n** (Supplementary Table S1) with isatin **4** and thiazolidine-4-carboxylic acid **5** in methanol under reflux for 2–3 h, as shown in Scheme 1. The new spiro-derivatives **6a-n** was fully characterized by FT-IR, ¹H- and ¹³C- NMR, and elemental analysis; spirooxindole analog **6i** was characterized by single-crystal x-ray diffraction analysis (data provided in SI, Supplementary Tables S1–S4). The stereochemistry and absolute configuration were assigned using experimental or theoretical approaches, and confirmed that the [3 + 2] cycloaddition (32CA) reaction proceeded via the *ortho/endo* pathway reaction mechanism (Scheme 2).

2.2 MEDT study of 32CA reaction between AY 7a and ethylene 3a

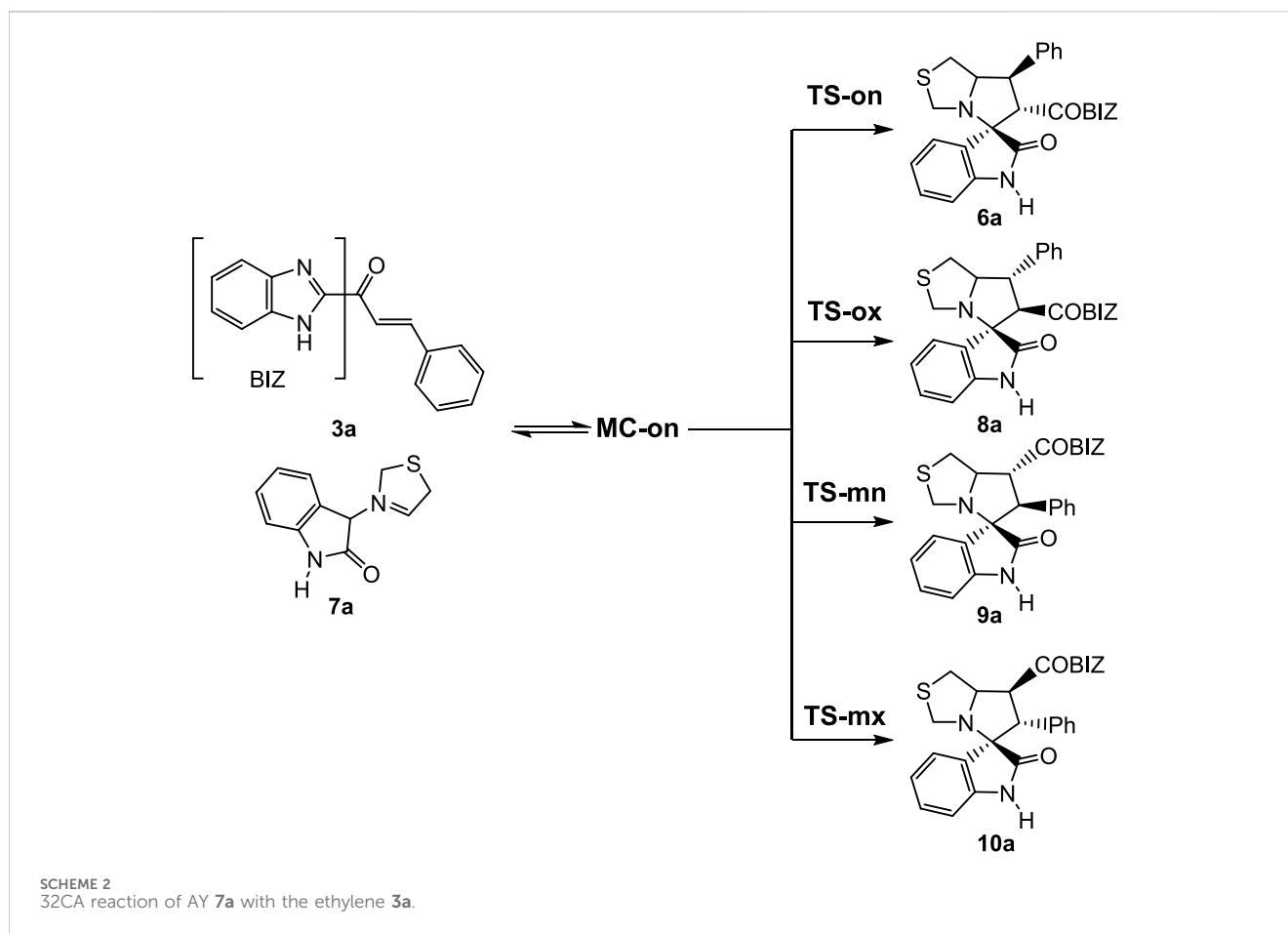
The 32CA reaction of AY **7a** with ethylene **3a** yielding *ortho/endo* spirooxindole **6a** was theoretically studied within the

Molecular Electron Density Theory (MEDT) (Domingo, 2016) to understand its behaviors (Scheme 2).

2.2.1 Study of 32CA reaction of AY **7a** with ethylene **3a**

Owing to the non-symmetry of both reagents, two pairs of *endo* and *exo* stereoisomeric and two pairs of *ortho* and *meta* regioisomeric reaction paths were studied (Scheme 2). Analysis of the stationary points found along the four reaction paths indicated that the 32CA reaction occurs through a one-step mechanism. ω B97X-D/6-311G(d,p) relative enthalpies and Gibbs free energies are presented in Table 1. The thermodynamic data are presented in Supplementary Table S7.

A series of molecular complexes (MCs) were also found, in which the two reagents were joined by weak intermolecular interactions. Only the most stable MC-**on** was selected as an energy reference. The distance between the two frameworks at this MC was ca. 3.2 Å; MC-**on** was 18.6 kcal·mol⁻¹ below the separated reagents (Table 1). Some conclusions can be drawn from the relative enthalpies in methanol given in Table 1: i) the most favorable TS-**on** was 11.7 kcal·mol⁻¹ below the separated reagents; if formation of MC-**on** is considered, the activation enthalpy becomes positive by 6.9 kcal·mol⁻¹; ii) this 32CA reaction is completely *endo* stereoselective as TS-**ox** was 5.7 kcal·mol⁻¹ above TS-**on**; iii) this 32CA reaction is completely *ortho* regioselective as TS-**mn** was 4.5 kcal·mol⁻¹ above TS-**on**. *Endo* stereoselectivity and *ortho* regioselectivity are in complete agreement



with the experimental outcomes; iv) this 32CA reaction was strongly exothermic as spirooxindole **6a** was $47.9 \text{ kcal}\cdot\text{mol}^{-1}$ below the separated reagents. Consequently, spirooxindole **6a** was formed via kinetic control.

The enthalpy and Gibbs free energy profiles associated with the four competitive reaction paths are shown in Figure 2. Inclusion of the thermal corrections and entropies to enthalpies increases the relative Gibbs free energies by $14.2\text{--}17.9 \text{ kcal}\cdot\text{mol}^{-1}$ as a consequence of the unfavorable relative entropies associated with this bimolecular process, which were between $-42.0 \text{ cal}\cdot\text{mol}^{-1}\cdot\text{K}^{-1}$ and $-52.9 \text{ cal}\cdot\text{mol}^{-1}\cdot\text{K}^{-1}$. Formation of **MC-on** was exergonic by $4.4 \text{ kcal}\cdot\text{mol}^{-1}$. The activation Gibbs free energy associated with the 32CA reaction of AY **7a** with ethylene **3a** via **TS-on** increased to $10.5 \text{ kcal}\cdot\text{mol}^{-1}$; formation of spirooxindole **6a** was exergonic by $31.5 \text{ kcal}\cdot\text{mol}^{-1}$. Considering the activation Gibbs free energies, this 32CA reaction is completely *endo* stereoselective and *ortho* regioselective as **TS-ox** and **TS-mn** are $4.7 \text{ kcal}\cdot\text{mol}^{-1}$ and $3.1 \text{ kcal}\cdot\text{mol}^{-1}$, respectively, above **TS-on** (Figure 2).

The geometries of the four TSs optimized in methanol are shown in Figure 3. The C–C distances between the four interacting carbons in the four TSs indicate that aside from the most unfavorable **TS-mx**, the other three TSs correspond to asynchronous C–C single-bond formation processes in which the shorter C–C distance corresponds to participation of the most electrophilic β -conjugated C4 carbon of ethylene **3a**. At the most favorable **TS-on**, the C–C distances

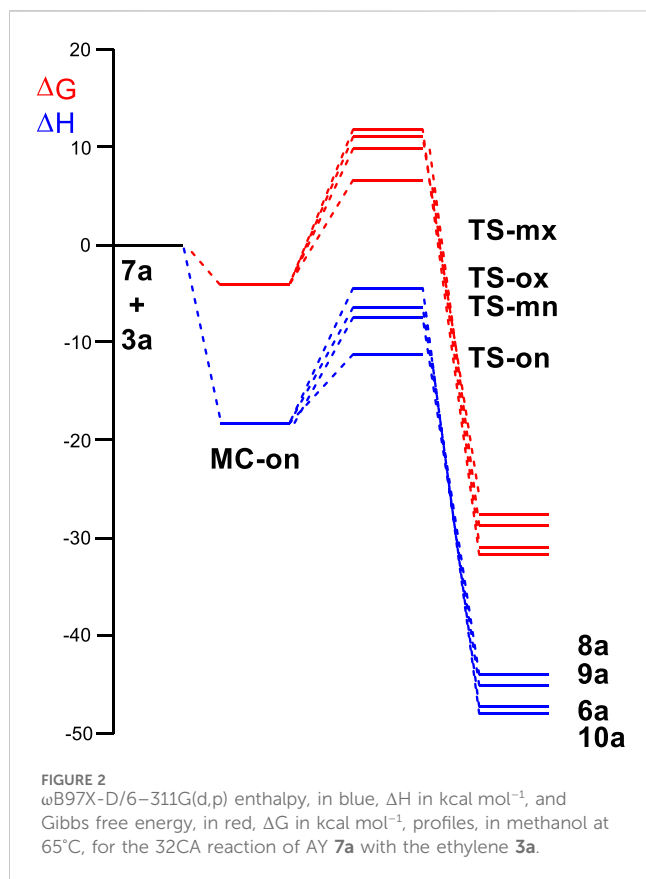
between the two pairs of interacting carbons, 2.137 \AA (C3–C4) and 2.757 \AA (C1–C5), indicate that this TS is associated with a high asynchronous C–C single-bond formation process. Analysis of the intrinsic reaction coordinates (IRC) (Fukui, 1970) associated with the highly asynchronous **TS-on** indicates that this 32CA reaction occurs through a non-concerted *two-stage one-step* mechanism (Domingo et al., 2008), in which the formation of the second C–C single bond begins after the first C–C single bond is completely formed.

Detailed analysis of the geometry of **TS-on** shows that one of the hydrogens of the benzene framework of ethylene **3a** is located at 2.484 \AA of the carbonyl oxygen of AY **7a**, and one hydrogen of the dihydrothiopyrrole ring of AY **7a** is located at 2.391 \AA of the carbonyl O7 oxygen of ethylene **3a** (Figure 3). These distances suggest the presence of two hydrogen bonds (HBs) between the hydrogen and oxygen centers. However, analysis of the geometry of the regioisomeric **TS-mn** shows the presence of only one HB between carbonyl O7 oxygen of ethylene **3a** and dihydrothiopyrrole hydrogen of AY **7a**, with H–O distances of 2.374 \AA (Figure 3).

Global electron density transfer (GEDT) analysis (Domingo, 2014) at the most favorable **TS-on** was used to assess the polar character of this 32CA reaction. GEDT values less than 0.05 e correspond to non-polar processes; values greater than 0.20 e correspond to polar processes. The high GEDT value found at

TABLE 1 ω B97X-D/6-311G(d,p) relative enthalpies (ΔH in kcal·mol⁻¹), entropies (ΔS in cal·mol⁻¹·K⁻¹), and Gibbs free energies (ΔG in kcal·mol⁻¹), with respect to the separated reagents, computed at 337.85 K and 1 atm in methanol, for the stationary points involved in the 32CA reaction of AY 7a with ethylene 3a.

	ΔH	ΔS	ΔG
MC-on	-18.6	-42.0	-4.4
MC-mn	-15.2	-37.9	-2.3
TS-on	-11.7	-52.9	6.1
TS-ox	-6.1	-50.1	10.9
TS-mn	-7.2	-48.6	9.2
TS-mx	-4.4	-46.5	11.4
6a	-47.9	-48.6	-31.5
8a	-44.2	-47.3	-28.3
9a	-45.1	-48.1	-28.8
10a	-48.3	-48.5	-31.9



TS-on (0.23 e), a consequence of the supernucleophilic character of AY 7a ($N = 4.39$ eV) and the strong nucleophilic character of ethylene 3a ($\omega = 2.39$ eV) (see Conceptual DFT (CDFT) analysis (Parr, 1983; Domingo et al., 2016) of the reagents in the Supplementary Material), indicates that this 32CA reaction is highly polar. The flux of the electron density, from AY 7a to ethylene 3a, classifies this 32CA reaction as a forward electron

density flux (FEDF) (Domingo et al., 2020), in agreement with the analysis of the CDFT indices.

2.2.2 What is the origin of the *ortho* regioselectivity?

Topological analysis of the electron localization function (ELF) (Becke and Edgecombe, 1990) of AY 7a showed the presence of two monosynaptic basins, $V(C1)$ and $V'(C1)$, integrating a total of 0.76 e at the C1 carbon, characterizing this three-atom-component as a *pseudo(mono)radical* species (Ríos-Gutiérrez et al., 2022) (Figure 4). Analysis of the nucleophilic P_k^- Parr functions (Domingo et al., 2013) of AY 7a indicates that the C1 carbon is more nucleophilic than the C3 carbon (see CDFT analysis of the reagents in the Supplementary Material). Consequently, the 32CA reaction of AY 7a with ethylene 3a is expected to be *meta* regioselective (Ríos-Gutiérrez et al., 2022).

A recent MEDT study on the unexpected *ortho* regioselectivity in the 32CA reactions of AYs derived from L-proline showed that the presence of two HBs at the MC-on, which are enhanced at the corresponding TS-on, can be responsible for the *ortho* regioselectivity of these 32CA reactions (Domingo et al., 2022).

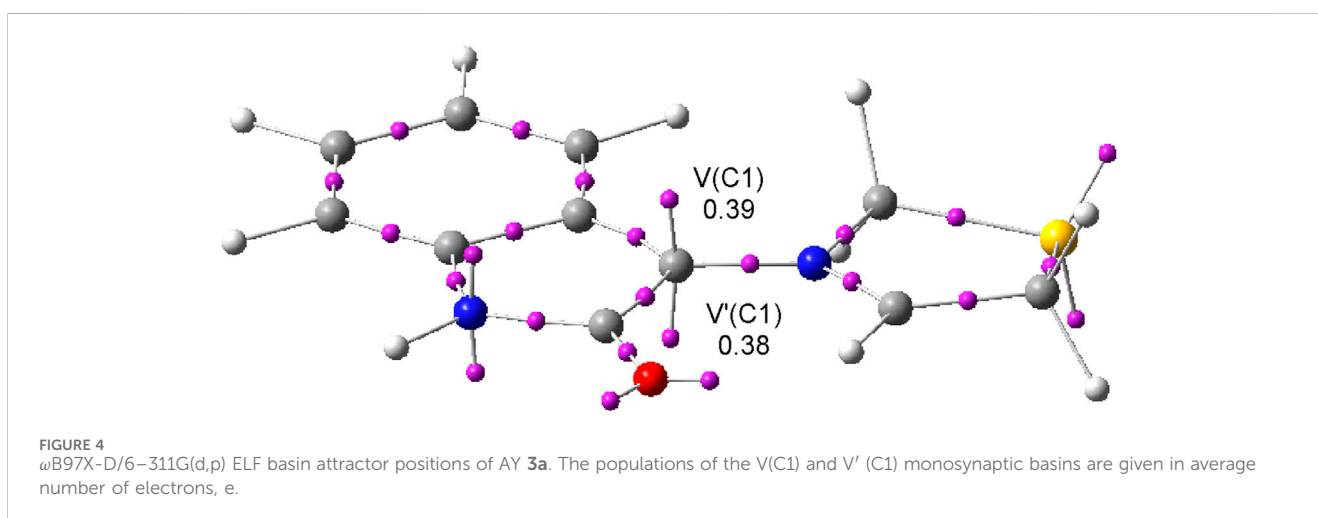
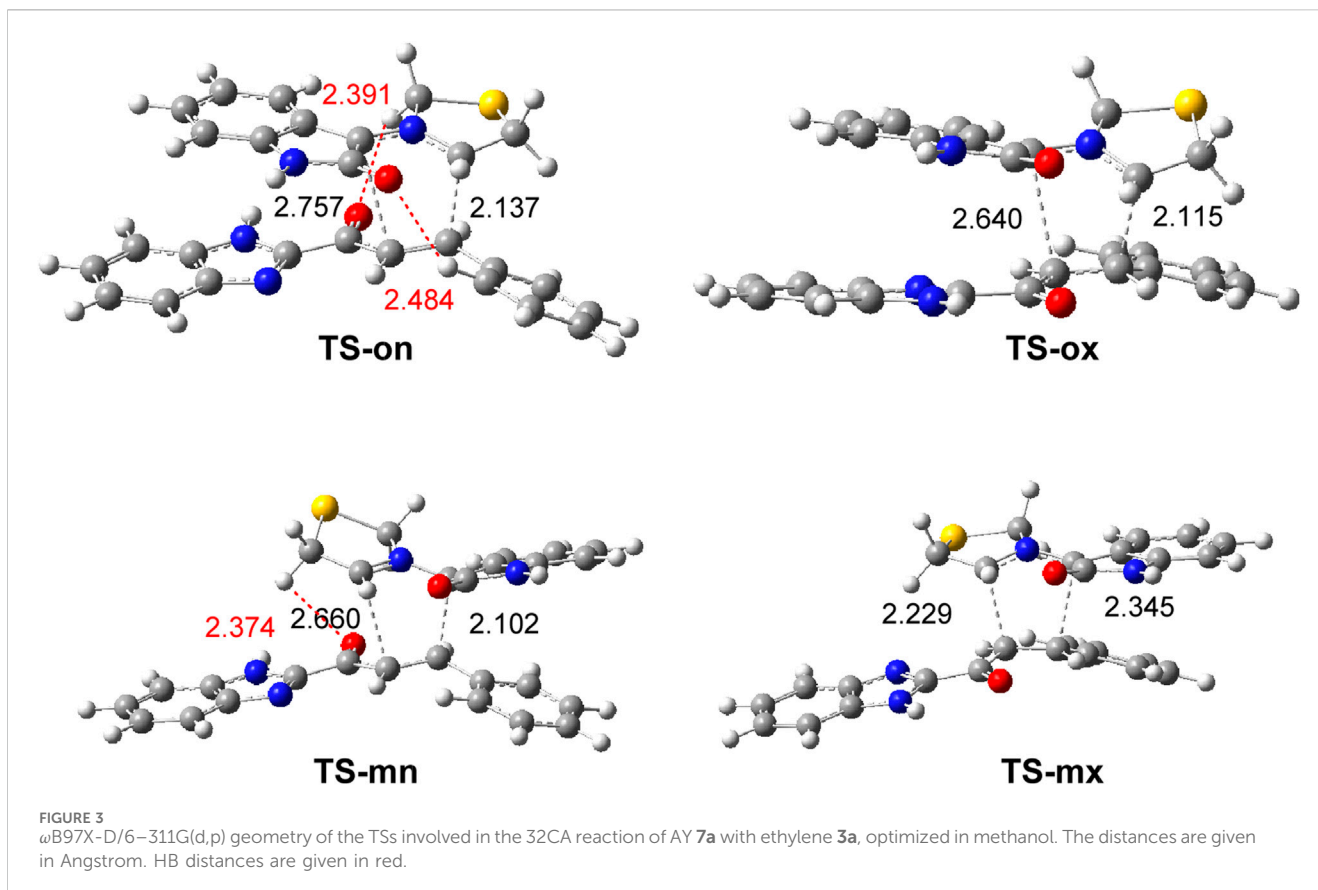
MC-on was 3.4 kcal mol⁻¹ more stable than MC-mn (Table 1). Analysis of the geometries of the two MCs shows the presence of an HB between one hydrogen of the CH₂ methylene continuous with the sulfur of AY 3a and the carbonyl O7 oxygen of ethylene 7a, with an O–H distance of 2.37 Å (Figure 5). MC-on shows an additional HB between a hydrogen of the aromatic ring of ethylene 3a and the oxygen atom of AY 7a, with an O–H distance of 2.69 Å (Figure 5). Formation of this HB required twisting of the benzene ring by 15.9°.

These two HBs, which are also present in the most stable TS-on (Figure 3), may account for the *ortho* and *endo* selectivity found in this 32CA reaction. The enthalpy difference between MC-on and MC-mn (3.4 kcal mol⁻¹) was increased to 4.5 kcal mol⁻¹ at the TSs as a consequence of stronger HB interactions.

An atom-in-molecules (AIM) (Richard et al., 1982) topological analysis of the electronic structure of the most favorable TS-on characterizes the two HBs responsive to the *ortho* reactions (see AIM topological analysis of the electronic structure of the most favorable TS-on in the Supplementary Material Table S6).

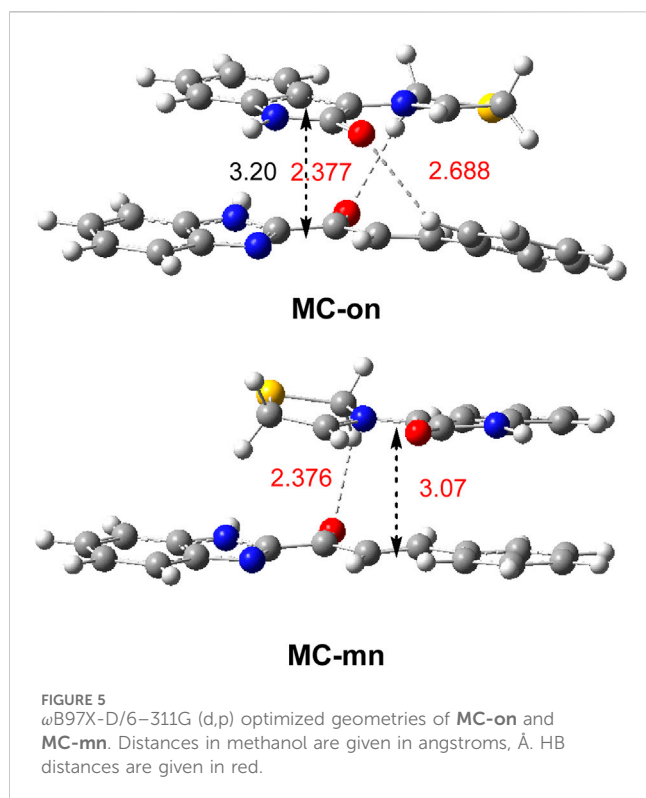
2.3 Biological evaluation and MTT assay

Initially, the target compounds of the spirooxindole analogs 6a–n were submitted to NCI for screening against 60 panels of cancer cells. Preliminary results showed promising feedback for the synthesized compounds of spirooxindole analogs (SI, Supplementary Table S8). For example, compounds 6a–n perfectly inhibited the growth of leukemia cells (CCRF-CEM; HL-60 (TB); K-562; MOLT-4; RPMI-8226, SR), with a GI% exceeding 80% except for compounds 6b, 6g, and 6l, which showed a smaller GI% (75%) for MOLT-4, RPMI-8226, and SR cancer cells. In non-small-cell lung cancer cells (A549/ATCC, EK VX, HOP-92, HOP62, NCI-H226, NCI-H23, NCI-H322M, NCI-H460, NCI-H460), the synthesized compounds showed complete growth inhibition, with the exception of 6g and 6l, which were the most reactive. We also observed that compounds 6g and 6l exhibited growth inhibition of less than 80% in CNS cancer cells (SF-268, SF-



295, SF-539, SNB-19, SNB-75, U251). The GI% of melanoma cells was completely inhibited by these compounds. For ovarian cancer cells (IGROVI), compounds **6b**, **6c**, **6d**, **6g**, and **6l** showed less reactivity, with a GI% from 55% to 75%. The other compounds showed excellent growth inhibition. For renal cancer cells (UO-31), the compounds exhibited less reactivity than with other renal cancer cells (786-0, A49, ACHN, CAKI-1, RXP393, SN12C, TK-10, DU-145). For breast cancer cells, complete growth inhibition was observed; however, compounds **6b-d**, **6g**, **6h**, and **6m** were less reactive against T-47D cancer cells, with a GI% between 54% and 80%.

The percentage of wi-38 viability and the growth inhibition percentages of MDA-MB231 and PC-3 cells after incubation with 5 μ M of different tested compounds were assessed using the MTT assay (Supplementary Table S9). From Supplementary Table S9, the viability of normal human lung cells (wi-38) exceeded 81% after incubation with 5 μ M of **6a** and **6d** compared to all other tested compounds, producing wi-38 cell death over 50%. The safest compound was **6a**, which did not affect the cell viability of wi-38 (-96%). Compounds **6a** and **6d** produced maximum viability on wi-38 and triggered death (>50%) in human cancer cells



(MDA-MB 231 and PC-3) (Supplementary Table S9). The values of the IC_{50} (μ M) of **6a–n** on Wi-38 viability and the growth of MDA-MB 231, and PC-3 cells are summarized in Table 2. This powerful anti-cancer effect was supported by severe morphological alterations (cell shrinkage and loss of normal spindle shape) in treated cancer cells compared with untreated cancer cells (Figure 6).

Figures 7A, B shows that **6a**- and **6d**-treated cancer cells demonstrated a higher percentage of annexin-stained cells than untreated cells. Furthermore, **6a** and **7d** induced apoptosis-dependent death (53.89%–55.34%) in treated breast- and prostate-cancer cell lines. This effect may be attributed to the potency of **6a** and **6d** for upregulating p21 expression by greater than three times and downregulating the expression level of cyclin D and NF- κ B in treated MDA-MB 231 cells compared to untreated cells (Figure 8). **6a** had the most significant effect on induction of p21 expression (5.3 times) and suppression of cyclin D and NF- κ B gene expression compared with **6d** ($p < 0.05$).

Figure 9A shows the immunohistochemistry results for the proliferation marker (Ki-67) and apoptosis marker (p53) in the MDA-MB 231 cell line after treatment for 72 h with **6a** and **6d**. These compounds reduced Ki-67 levels (from 82.425% to 1.18% and 3.03%, respectively), as indicated by the increase in purple-stained cells in comparison with brown-stained untreated control cells (Figures 9AI, III). Figures 9AII, III show that **6a** and **6d** increased the protein levels of p53 by 60.2% and 54.7%, respectively, compared to the untreated MDA-MB 231 cells, which mostly lacked brown p53-nuclear staining. Moreover, the active p53 transcription factor was assessed in the treated MDA-MB 231 cells compared to untreated cells by quantifying the p53 bound to a target oligonucleotide-coated plate. Both compounds exhibited

high efficiency for p53 activation, 5.983 ± 0.142 and 6.287 ± 0.254 , respectively (Figure 9B). This may be due to their inhibitory potency against MDM2, which limits its degradation.

Some of the synthesized spirooxindoles based on benzimidazole were selected for further MDM2 binding affinity using the MST assay. The results are summarized in Table 3; the binding curve is presented in the Supplementary Information. Compounds **6a**, **6b**, **6d**, **6e**, **6h**, **6i**, and **6l** exhibited moderate to excellent binding affinity with the MDM2 receptor, with a range of $K_D = 6.68$ – 113μ M (SI; Supplementary Figures S3–S9). The most active compound was **6h** ($K_D = 6.68 \mu$ M); the spirooxindole-based benzimidazole had a benzene ring with a hydroxyl group in the *meta*-position for further binding interaction with the key amino acid. Having electron-donating groups such as methyl or trimethoxy groups on the benzene ring (**6d** and **6i**) showed good binding, with $K_D = 17.4 \mu$ M and 21μ M, respectively. However, the presence of halogens such as chlorine or bromine atoms decreased the binding affinity with MDM2 to 38.2μ M and 49.9μ M for compounds **6b** and **6l**, respectively. Without any substitution on the benzene ring (compound **6a**) or change to a heterocycle such as thiophene (compound **6e**), the least reactivity toward binding with the protein receptor was observed.

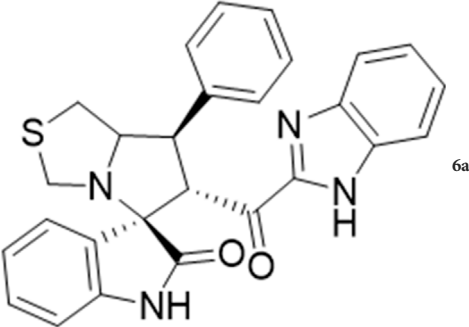
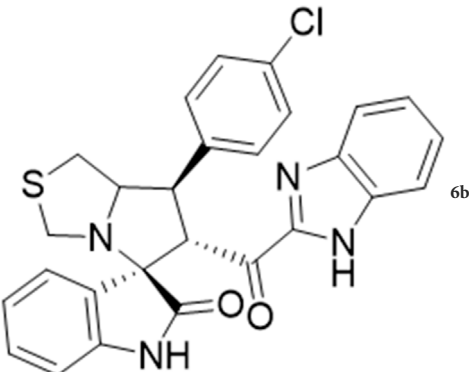
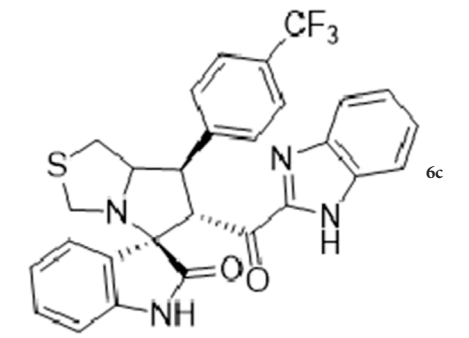
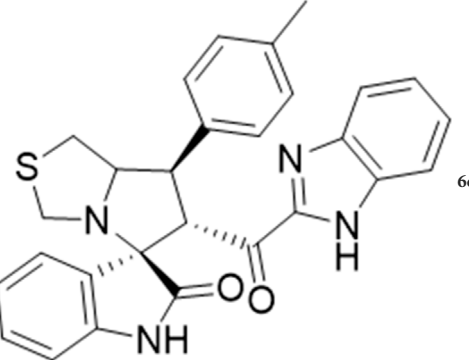
2.4 Molecular docking study

The designed compounds (**6a–l**) and standard co-crystallized spirooxindole compounds were docked with the MDM2 protein, which was retrieved from the Protein Data Bank (PDB code: 5law) (Gollner et al., 2016a). The docking protocol was performed using OpenEye scientific software (Docking, 2016). To validate the docking protocol, the standard ligand **6SJ** was re-docked with the receptor. The standard ligand **6SJ** exhibited the same binding mode and pose as its co-crystallized complex (Gollner et al., 2016a), completely overlaying each other, as shown in Figure 10A. It formed HBs with Leu:54AA through the NH of the indole and with Lys:94AA through the protonated nitrogen of the pyrrolidine amino acid. Compound **6h** exhibited high similarity in binding pose and mode with the co-crystallized ligand (Figure 10B). It interacts with the receptor through formation of HBs with Leu:54AA through the NH of the indole, and with Lys:94AA through phenolic functionality. Figure 10C shows the deposition of compound **6d** inside the active receptor domains. The compound interacted with its receptor via hydrophobic interactions. Figure 10D shows the docking pose and mode of compound **6d** compared with those of the standard ligand **6SJ**. The benzimidazole ring of compound **6d** was overlaid with the indole moiety of the standard ligand **6SJ**. However, the remaining features of both compounds were oriented in different directions.

2.5 Shape alignment and ROCS analysis

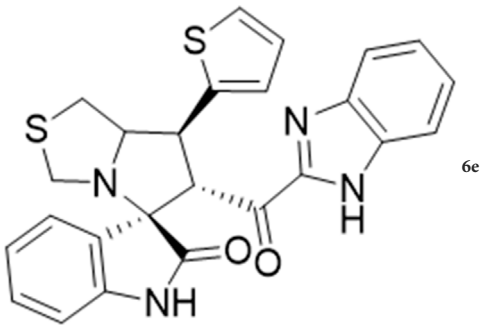
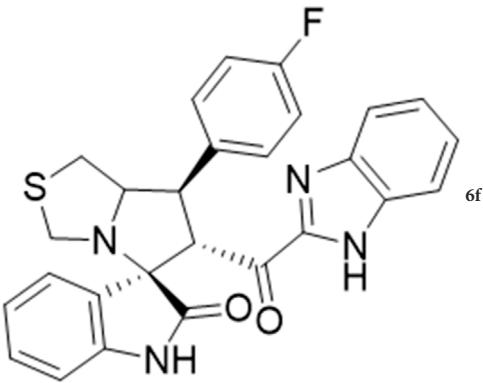
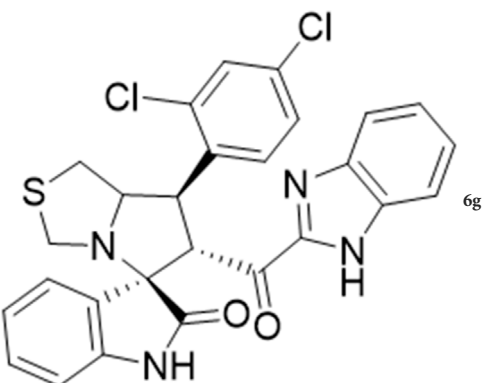
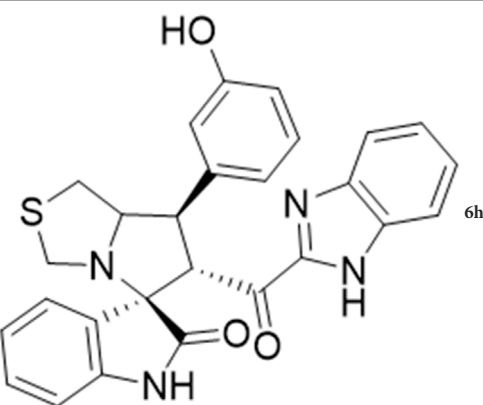
The rapid overlay chemical similarity (ROCS) approach was used to determine compound similarity based on 3D structures and automated crafted descriptors using OpenEye software. Shape similarity was determined using Tanimoto scores. The Tanimoto Combo (maximum value = 2) is the sum of the shape (maximum

TABLE 2 The estimated IC₅₀ (μM) of 6a-n on Wi-38 viability and the growth of MDA-MB 231, and PC-3 cells.

Chemical structure	Wi-38	MDA-MB 231	PC-3
	IC ₅₀ (μM)		
 6a	22.163 ± 1.586	2.968 ± 0.047	4.107 ± 0.167
 6b	4.962 ± 0.117	4.757 ± 0.265	4.819 ± 0.000
 6c	12.887 ± 1.512	3.341 ± 0.210	4.151 ± 0.232
 6d	5.180 ± 0.138	4.303 ± 0.137	4.294 ± 0.054

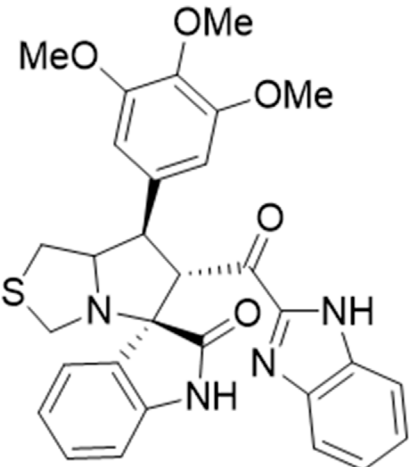
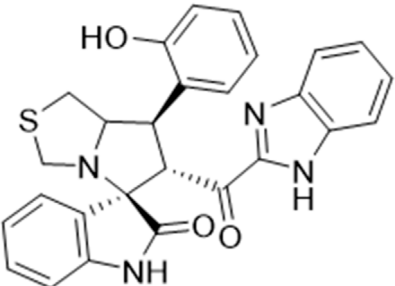
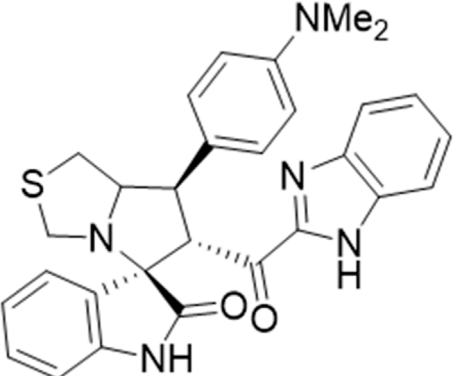
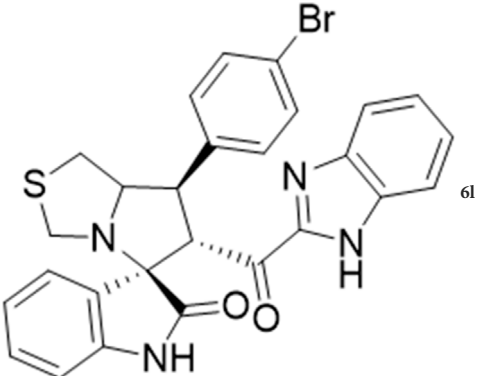
(Continued on following page)

TABLE 2 (Continued) The estimated IC₅₀ (μM) of 6a-n on Wi-38 viability and the growth of MDA-MB 231, and PC-3 cells.

Chemical structure	Wi-38	MDA-MB 231	PC-3
	IC ₅₀ (μM)		
 <p>6e</p>	4.752 ± 0.008	5.605±	5.432 ± 0.098
 <p>6f</p>	4.166 ± 0.076	4.407 ± 0.448	4.593 ± 0.132
 <p>6g</p>	5.106 ± 0.191	6.216 ± 0.000	6.191 ± 0.191
 <p>6h</p>	4.408 ± 0.07	5.442 ± 0.167	5.041 ± 0.316
	4.081 ± 0.201	6.680 ± 0.463	6.017 ± 0.106

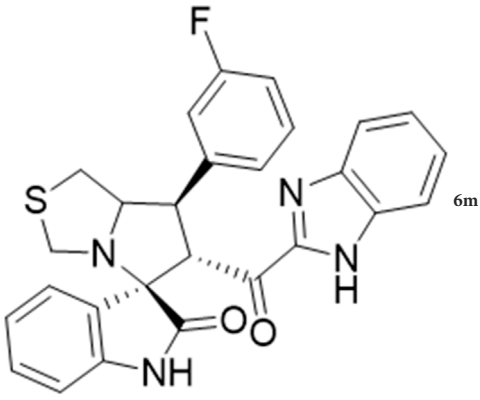
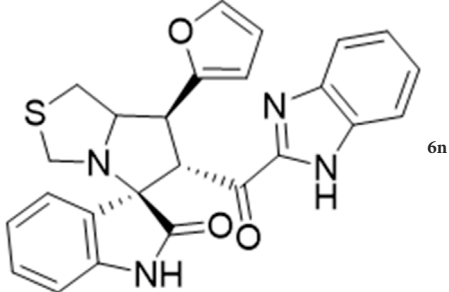
(Continued on following page)

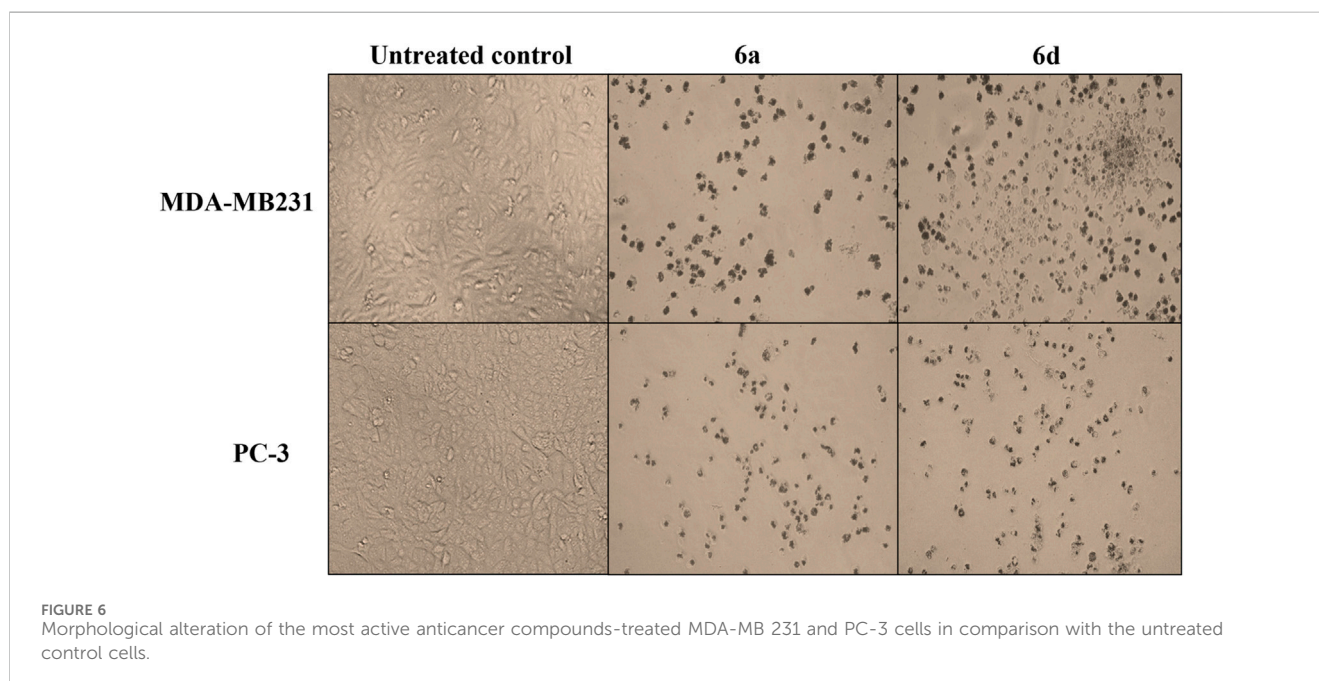
TABLE 2 (Continued) The estimated IC₅₀ (μM) of 6a-n on Wi-38 viability and the growth of MDA-MB 231, and PC-3 cells.

Chemical structure	Wi-38	MDA-MB 231	PC-3
	IC ₅₀ (μM)		
 <p>6i</p>			
 <p>6j</p>	3.998 ± 0.129	4.665 ± 0.009	4.543 ± 0.163
 <p>6k</p>	3.950 ± 0.319	3.995 ± 0.249	4.160 ± 0.036
 <p>6l</p>	6.259 ± 0.443	4.510 ± 0.203	4.627 ± 0.116
	4.650 ± 0.127	4.733 ± 0.224	4.766 ± 0.132

(Continued on following page)

TABLE 2 (Continued) The estimated IC₅₀ (μM) of 6a-n on Wi-38 viability and the growth of MDA-MB 231, and PC-3 cells.

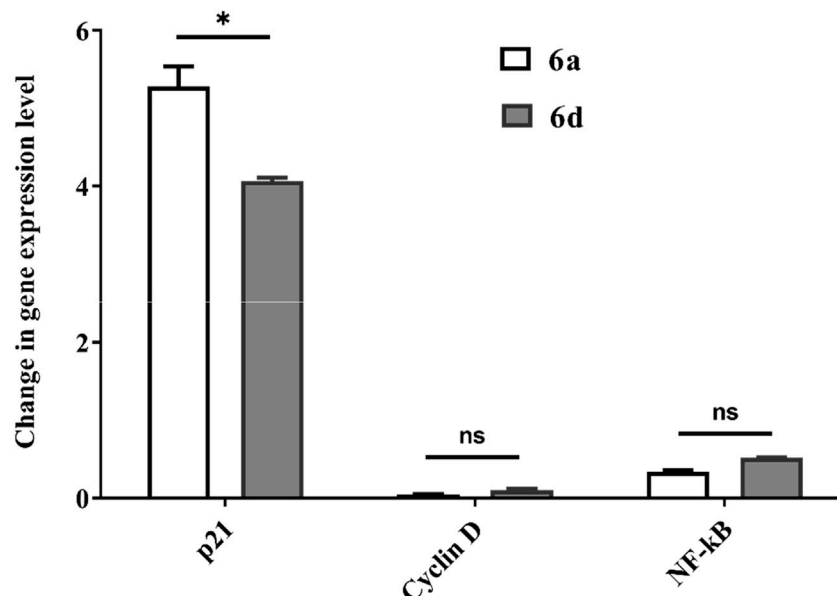
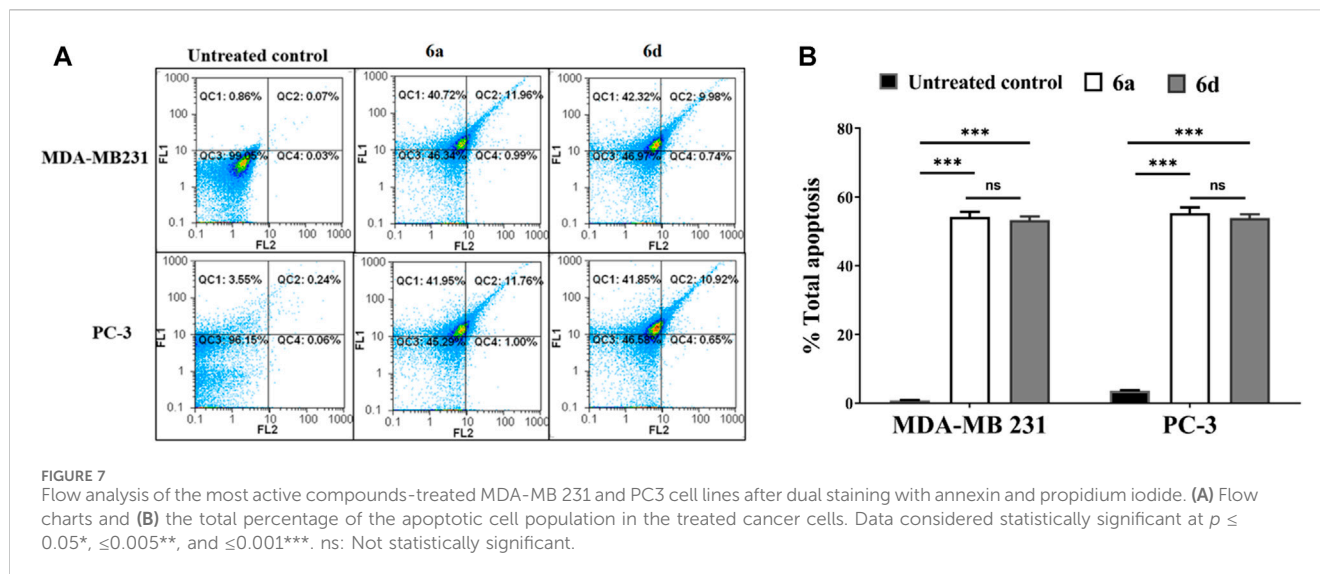
Chemical structure	Wi-38	MDA-MB 231	PC-3
	IC ₅₀ (μM)		
 6m			
 6n	4.171 ± 0.166	6.143 ± 0.246	6.247 ± 0.533



value = 1) and color (maximum value = 1) Tanimoto scores. Considering **6SJ**, compound score was not correlated to activity. Compounds **6d** and **6h** had TC scores of 0.83 and 0.81, respectively, as shown in Table 4. The results indicated that our scaffolds could resemble another target or have unique chemometric characteristics.

For compounds **6d** and **6h**, the color and shape atoms (generated by the ROCS application, OpenEye software) are shown in Figures 11A–C compared with the standard ligand (**6SJ**).

The most important descriptors for compounds **6d** and **6h** are presented in Table 5, compared with the **6SJ** standard. Both

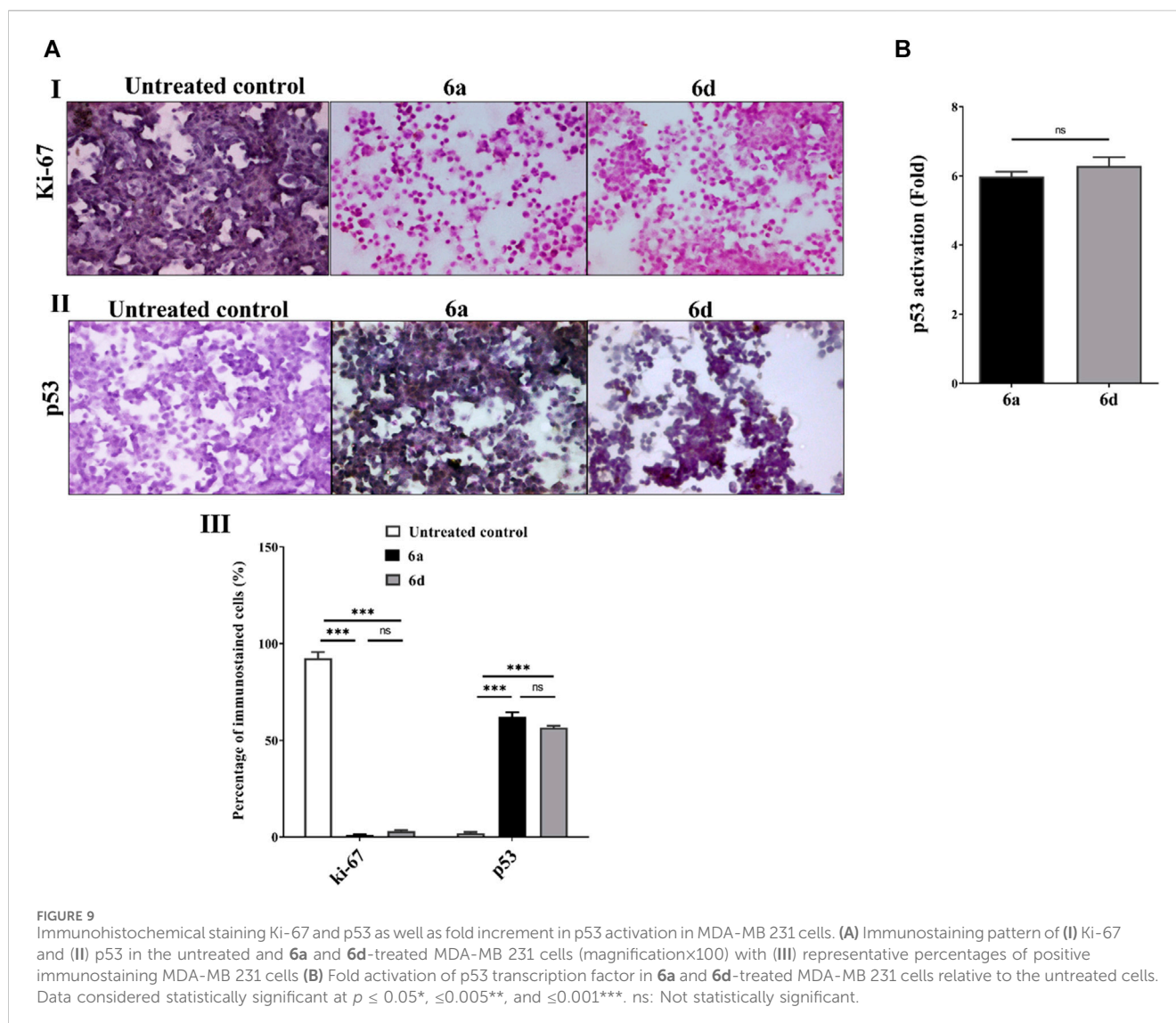


compounds showed values similar to the standard; however, the number of rotatable bonds was three in compounds **6d** and **6h** and five in **6SJ**. These results highlight the importance of the number of rotatable bonds, as previously reported (Abdelhady et al., 2022).

3 Structure activity relationship

For MDM2 binding, compound **6h** showed stronger binding activity than **6d**, **6i**, **6b**, **6l**, **6a**, and **6e**. The electronic positions of the substituents on the phenyl rings of the benzaldehyde derivatives contributed in both the electronic and geometric

properties of the final scaffolds. Compound **6h** contained a phenolic OH group at the meta position and formed a HB with Lys:94AA in the receptor. Furthermore, compound **6h** showed a unique orientation inside the receptor; none of the compounds overlapped with it. Compound **6d**, with a mildly activating group (Me) at the para position, showed low Log p and PSA values (Table 5). The PSA level was similar to that of **6SJ**. Compounds with electron-withdrawing groups, namely, *p*-Cl and *p*-Br, and thiophene moieties, exhibited lower activity, probably due to the electronic effect of the compound topology. The meta-position with formation of an extra HB was preferable for inhibitory activity (SI, Supplementary Figure S10).



3.1 Experimental

3.1.1 General

“All chemicals were purchased from Aldrich, Sigma-Aldrich, and Fluka, and were used without further purification unless otherwise indicated. All melting points were measured using a Gallenkamp melting point apparatus in open glass capillaries and were uncorrected. The crude products were purified using silica gel through column chromatography (100–200 mesh). IR spectra were recorded as KBr pellets using a Nicolet 6700 FT-IR spectrophotometer. NMR spectra were recorded using a Varian Mercury Jeol-400 NMR spectrometer. ^1H NMR (400 MHz) and ^{13}C NMR (100 MHz) spectroscopy were performed in either deuterated dimethyl sulfoxide ($\text{DMSO}-d_6$) or deuterated chloroform (CDCl_3) (SI; Supplementary Figures S11–23). Chemical shifts (δ) are reported in ppm; coupling constant J is given in Hz. Elemental analysis was performed using an Elmer 2400 Elemental Analyzer in CHN mode. Chalcones **3a–n** was prepared as reported previously by (Alshahrani et al., 2023)”.

3.1.2 General procedure for synthesis of spiro compounds (6a–n)

A mixture of chalcone derivative **3a–n** (0.5 mmol), thiazolidine-4-carboxylic acid (66.59 mg, 0.5 mmol), and isatin (73.57 mg, 0.5 mmol) in methanol (20 ml) was stirred at 60–65°C in an oil bath for 2–3 h. The final spirooxindole-based benzimidazole was separated using either by filtration if the final product precipitated or by column chromatography ((Silica Gel 60, granulometry 0.015–0.040 mm, Merck); eluent: EtOAc/nHexane gradient polarity according to the specified compound starting from 30:70 until 50:50).

3.1.3 (3*S*,6'*R*)-6'-(1*H*-benzo [d]imidazole-2-carbonyl)-7'-phenyl-3',6',7',7a'-tetrahydro-1'*H*-spiro [indoline-3.5'-pyrrolo [1,2-*c*]thiazol]-2-one (6a)

White solid; yield (89%); m.p: 240°C–242°C; IR (KBr, cm^{-1}): 3432 (NH), 3276 (NH), 3094 (CH), 2934 (CH), 1732 (CO), 1684 (CO); ^1H -NMR (400 MHz, $\text{DMSO}-d_6$): δ 12.95 (1H, s, NH), 10.39 (1H, s,

TABLE 3 MST binding assay results of MDM2.

#	Code	Chemical structures	K_D (μM)
1	6a		87.7
2	6b		38.2
3	6d		17.4
4	6e		113
5	6h		6.68
6	6i		21

(Continued in next column)

TABLE 3 (Continued) MST binding assay results of MDM2.

#	Code	Chemical structures	K_D (μM)
7	6l		49.9

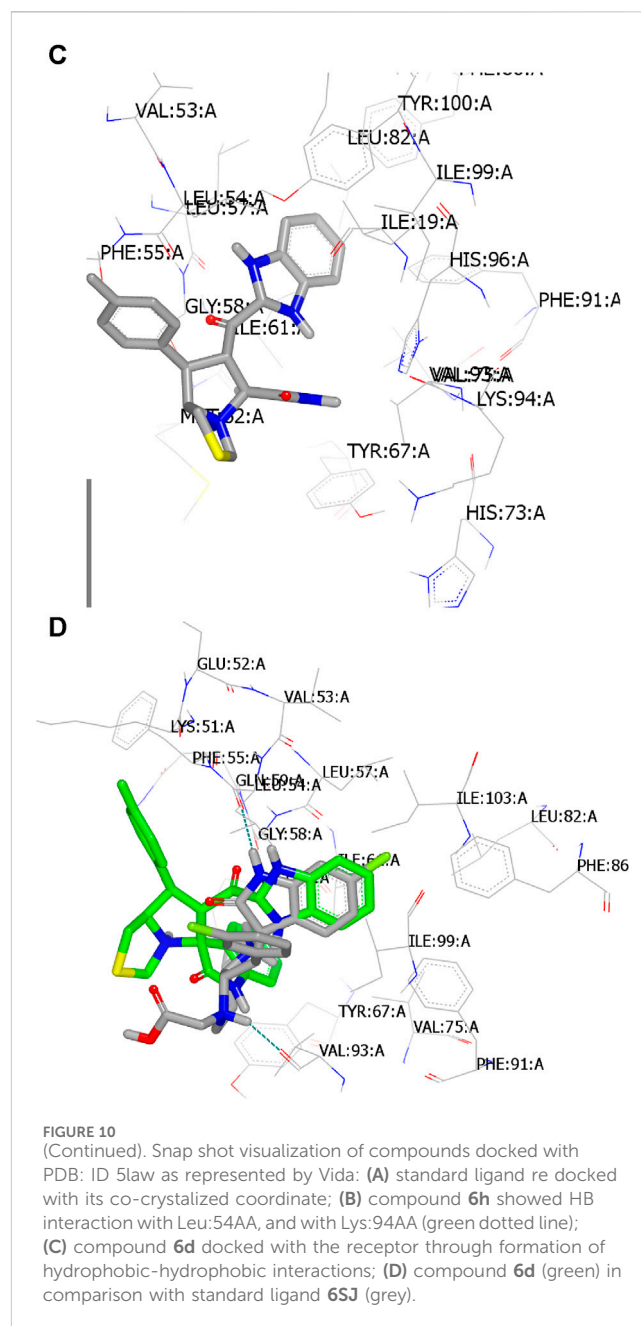
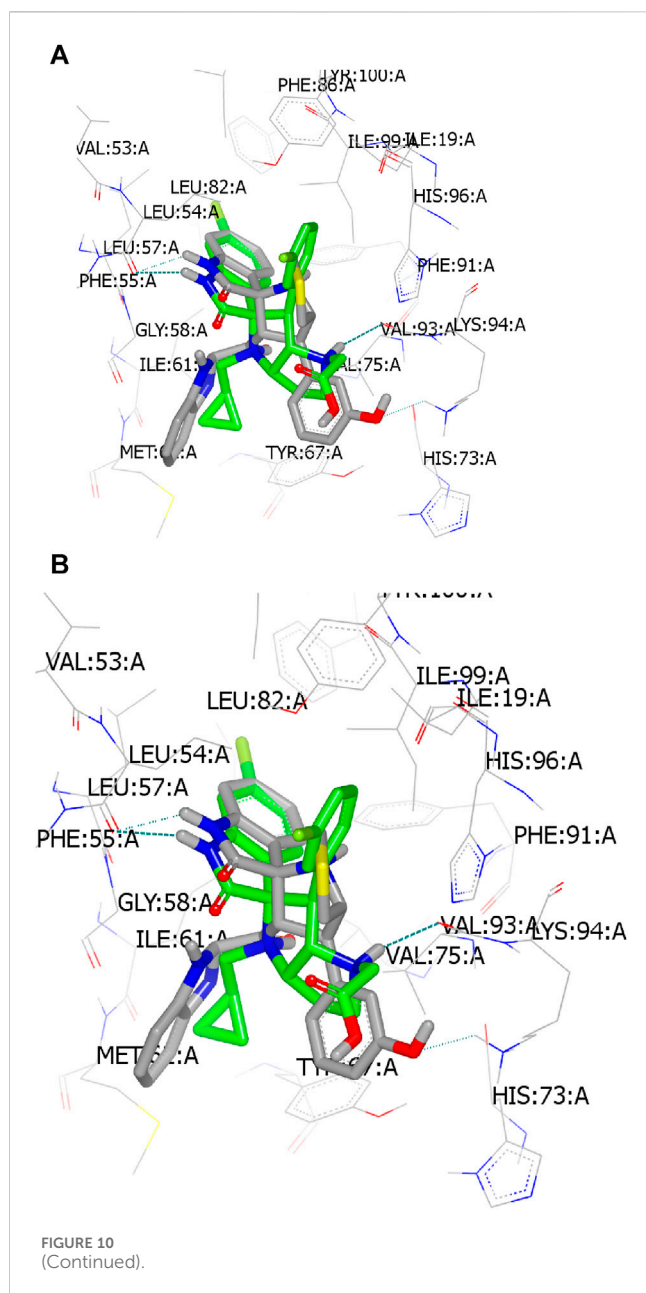
NH), 7.69 (1H, d, $J = 8$ Hz, ArH), 7.50 (2H, d, $J = 8$ Hz, ArH), 7.38–7.18 (7H, m, ArH), 6.99 (1H, t, $J = 8$ Hz, ArH), 6.84 (1H, t, $J = 8$ Hz, ArH), 6.44 (1H, d, $J = 8$ Hz, ArH), 5.17 (1H, d, $J = 11.2$ Hz, CHCO), 4.26 (1H, q, $J = 8$ Hz, CHN), 3.94 (1H, t, $J = 10.2$ Hz, CHPh), 3.68 (1H, d, $J = 8.8$ Hz), 3.40 (1H, d, $J = 8.4$ Hz), 3.18 (2H, d, $J = 5.2$ Hz), 2.98 (2H, dd, $J = 19.2, 5.3$ Hz); $^{13}\text{C-NMR}$ (101 MHz, DMSO- d_6): δ 190.05, 178.85, 147.94, 143.19, 142.94, 140.21, 135.11, 129.41, 128.55, 127.64, 124.31, 122.07, 113.19, 109.89, 74.51, 72.44, 63.53, 51.82, 50.08, 35.28; Anal. for $\text{C}_{27}\text{H}_{22}\text{N}_4\text{O}_2\text{S}$; calcd: C, 69.51; H, 4.75; N, 12.01; O, 6.86; S, 6.87; Found: C, 69.49; H, 4.77; N, 12.04; O, 6.82; S, 6.88.

3.1.4 (3S,6'R)-6'-(1H-Benzo [d]imidazole-2-carbonyl)-7'-(4-chlorophenyl)-3',6',7',7a'-tetrahydro-1'H-spiro [indoline-3.5'-pyrrolo [1,2-c]thiazol]-2-one (6b)

Pale yellow solid; yield (57%); m.p.: 210–212°C; IR (KBr, cm^{-1}): 3434 (NH), 3277 (NH), 3093 (CH), 2929 (CH), 1729 (CO), 1682 (CO); $^1\text{H-NMR}$ (400 MHz, DMSO- d_6): δ 12.96 (1H, s, NH), 10.41 (1H, s, NH), 7.54 (3H, d, $J = 8$ Hz, ArH), 7.41 (3H, d, $J = 8$ Hz, ArH), 7.23 (3H, d, $J = 7.3$ Hz, ArH), 6.98 (1H, t, $J = 7.6$ Hz, ArH), 6.82 (1H, t, $J = 7.6$ Hz, ArH), 6.44 (1H, d, $J = 7.8$ Hz, ArH), 5.12 (1H, d, $J = 11$ Hz, CHCO), 4.23 (1H, q, $J = 8$ Hz, CHN), 3.95 (1H, t, $J = 10$ Hz, CHPh), 3.67 (1H, d, $J = 8.8$ Hz), 3.39 (2H, d, $J = 8.8$ Hz), 2.98 (2H, m); $^{13}\text{C-NMR}$ (101 MHz, DMSO- d_6): δ 189.91, 178.79, 147.91, 143.23, 139.26, 132.41, 130.42, 129.30, 124.23, 121.36, 109.96, 74.32, 72.35, 63.16, 49.17, 35.10, 27.77; Anal. for $\text{C}_{27}\text{H}_{21}\text{ClN}_4\text{O}_2\text{S}$; calcd: C, 64.73; H, 4.22; Cl, 7.08; N, 11.18; O, 6.39; S, 6.40; Found: C, 64.69; H, 4.27; Cl, 7.06; N, 11.20; O, 6.35; S, 6.43.

3.1.5 (3S,6'R)-6'-(1H-Benzo [d]imidazole-2-carbonyl)-7'-(4-(trifluoromethyl) phenyl)-3',6',7',7a'-tetrahydro-1'H-spiro [indoline-3.5'-pyrrolo [1,2-c]thiazol]-2-one (6c)

Yellow solid; yield (13.5%); m.p.: 185–187°C; IR (KBr, cm^{-1}): 3429 (NH), 3282 (NH), 3099 (CH), 2927 (CH), 1724 (CO), 1686 (CO); $^1\text{H-NMR}$ (CDCl_3 , 400 MHz): δ 12.90 (1H, s, NH), 10.42 (1H, s, NH), 7.45 (2H, d, $J = 8$ Hz, ArH), 7.23 (4H, d, $J = 8$ Hz, ArH), 7.08 (1H, d, $J = 8$, ArH), 6.98 (1H, t, $J = 7.7$ Hz, ArH), 6.90 (1H, t, $J = 7.7$ Hz, ArH), 6.84 (1H, d, $J = 7.3$ Hz, ArH), 6.45 (2H, t, $J = \text{Hz}$, ArH), 5.16 (1H, d, $J = \text{Hz}$, CHCO), 4.24 (1H, q, $J = \text{Hz}$, CHN), 4.06 (1H, t, $J = \text{Hz}$, CHPh), 3.68 (2H, d, $J = 8.8$ Hz), 3.25 (1H, d, $J = 12$ Hz), 3.00 (2H, m); Anal. for $\text{C}_{28}\text{H}_{21}\text{F}_3\text{N}_4\text{O}_2\text{S}$; calcd: C, 62.91; H, 3.96; F, 10.66; N, 10.48; O, 5.99; S, 6.00; Found: C, 62.96; H, 3.92; F, 10.67; N, 10.42; O, 6.01; S, 6.02.



3.1.6 (3*S*,6'*R*)-6'-(1*H*-Benzo [*d*]imidazole-2-carbonyl)-7'-(*p*-tolyl)-3',6',7',7*a*'-tetrahydro-1'*H*-spiro [indoline-3.5'-pyrrolo [1,2-*c*]thiazol]-2-one (**6d**)

White solid; yield (66%); m.p.:228–230°C; IR (KBr, cm⁻¹): 3649 (NH), 3277 (NH), 3087(CH), 2926 (CH), 1727 (CO), 1690 (CO); ¹H-NMR (400 MHz, DMSO-*d*₆): δ 12.94 (1H, s, NH), 10.37 (1H, s, NH), 7.69 (1H, d, *J* = Hz, ArH), 7.38–7.20 (6H, m, ArH), 7.15 (2H, d, *J* = Hz ArH), 6.99 (1H, t, *J* = 7.6 Hz, ArH), 6.84 (1H, t, *J* = 7.6 Hz, ArH), 6.44 (1H, d, *J* = 7.8 Hz, ArH), 5.15 (1H, d, *J* = 11.3 Hz, CHCO), 4.20 (1H, q, *J* = 8 Hz, CHN), 3.88 (1H, t, *J* = 10.6 Hz, CHPh), 3.67 (1H, d, *J* = 8.8 Hz), 3.39 (2H, d, *J* = 8.8 Hz), 3.18 (1H, d, *J* = 5.1 Hz), 2.96 (2H, m), 2.23 (3H, s, CH₃); ¹³C-NMR (101 MHz, DMSO-*d*₆): δ 190.08, 178.84, 147.98, 143.16, 142.96, 137.03, 136.93, 135.10, 130.01, 128.37, 127.49, 126.34, 124.35, 123.43, 122.00, 121.94, 121.37, 113.28, 109.93, 74.49, 72.44, 63.24, 51.84, 49.89, 35.25, 21.23; Anal. for C₂₈H₂₄N₄O₂S; calcd: C,

69.98; H, 5.03; N, 11.66; O, 6.66; S, 6.67; Found: C, 69.95; H, 5.06; N, 11.68; O, 6.63; S, 6.68.

3.1.7 (3*S*,6'*R*)-6'-(1*H*-Benzo [*d*]imidazole-2-carbonyl)-7'-(thiophen-2-yl)-3',6',7',7*a*'-tetrahydro-1'*H*-spiro [indoline-3.5'-pyrrolo [1,2-*c*]thiazol]-2-one (**6e**)

White solid; yield (76%); m.p.:240–242°C; IR (KBr, cm⁻¹): 3624 (NH), 3258 (NH), 3091(CH), 2927 (CH), 1728 (CO), 1689 (CO); ¹H-NMR (400 MHz, DMSO-*d*₆): δ 13.02 (1H, s, NH), 10.35 (1H, s, NH), 7.71 (1H, d, *J* = 8 Hz, ArH), 7.40 (1H, d, *J* = 5.1 Hz, CHS), 7.37–7.21 (4H, m, ArH), 7.12 (1H, d, *J* = 3.5 Hz, ArH), 7.04–6.94 (2H, m, ArH), 6.84 (1H, t, *J* = 7.5 Hz, ArH), 6.44 (1H, d, *J* = 7.5 Hz, ArH), 5.07 (1H, d, *J* = 10.3 Hz, CHCO), 4.25–4.18 (2H, m), 3.68 (1H, d, *J* = 9.3 Hz), 3.39 (1H, d, *J* = 9.1 Hz), 3.21–3.01 (4H, m); ¹³C-NMR (101 MHz,

TABLE 4 Tanimoto combo scores of designed compounds using 6SJ standard as ShapeQuery.

Vida name	Tanimoto combo	Shape tanimoto	Color tanimoto
6sj law standard	2	1	1
6n	0.902	0.658	0.244
6j	0.882	0.663	0.219
6e	0.843	0.634	0.209
6m	0.835	0.626	0.209
6d	0.834	0.625	0.209
6h	0.819	0.627	0.192
6a	0.816	0.598	0.218
6k	0.806	0.598	0.209
6b	0.805	0.587	0.218
6g	0.799	0.580	0.218
6l	0.797	0.588	0.209
6c	0.789	0.580	0.209
6i	0.710	0.535	0.175

DMSO- d_6): δ 189.66, 178.54, 147.84, 143.13, 143.00, 142.76, 135.15, 130.26, 127.66, 126.00, 124.01, 113.42, 109.93, 74.31, 72.66, 63.78, 52.25, 45.39, 35.45; Anal. for $C_{25}H_{20}N_4O_2S_2$; calcd: C, 63.54; H, 4.27; N, 11.86; O, 6.77; S, 13.57; Found: C, 63.49; H, 4.24; N, 11.84; O, 6.80; S, 13.63.

3.1.8 (3*S*,6'*R*)-6'-(1*H*-Benzo [d]imidazole-2-carbonyl)-7'-(4-fluorophenyl)-3',6',7',7a'-tetrahydro-1'*H*-spiro [indoline-3.5'-pyrrolo [1,2-*c*]thiazol]-2-one (6f)

White solid; yield (31%); m.p.:233–235°C; IR (KBr, cm^{-1}): 3431 (NH), 3268 (NH), 3096 (CH), 2960 (CH), 1732 (CO), 1684 (CO); 1H -NMR (400 MHz, DMSO- d_6): δ 12.95 (1H, s, NH), 10.39 (1H, s, NH), 7.68 (1H, d, J = 8 Hz, ArH), 7.54 (2H, t, J = 6.8 Hz, ArH), 7.36–7.14 (6H, m, ArH), 6.98 (1H, t, J = 7.7 Hz, ArH), 6.83 (1H, t, J = 7.7 Hz, ArH), 6.43 (1H, d, J = 7.4 Hz, ArH), 5.11 (1H, d, J = 11 Hz, CHCO), 4.20 (1H, q, J = 9.6 Hz, CHN), 3.95 (1H, t, J = 10.3 Hz, CHPh), 3.67 (1H, d, J = 8.8 Hz), 3.40 (1H, d, J = 12 Hz), 2.98 (2H, m); ^{13}C -NMR (101 MHz, DMSO- d_6): δ 189.97, 178.79, 169.71, 147.90, 143.21, 135.10, 130.23, 124.24, 72.33; Anal. for $C_{27}H_{21}FN_4O_2S$; calcd C, 66.93; H, 4.37; F, 3.92; N, 11.56; O, 6.60; S, 6.62; Found: C, 66.97; H, 4.34; F, 3.94; N, 11.53; O, 6.63; S, 6.59.

3.1.9 (3*S*,6'*R*)-6'-(1*H*-Benzo [d]imidazole-2-carbonyl)-7'-(2,4-dichlorophenyl)-3',6',7',7a'-tetrahydro-1'*H*-spiro [indoline-3.5'-pyrrolo [1,2-*c*]thiazol]-2-one (6g)

White solid; yield (38%); m.p.:235–237°C; IR (KBr, cm^{-1}): 3436 (NH), 3281 (NH), 3090 (CH), 2925 (CH), 1730 (CO), 1685 (CO); 1H -NMR (400 MHz, DMSO- d_6): δ 12.96 (1H, s, NH), 10.44 (1H, s, NH), 7.85 (1H, d, J = 8.5 Hz, ArH), 7.69 (1H, d, J = 8 Hz, ArH), 7.63 (1H, s, ArH), 7.51 (1H, d, J = 8 Hz, ArH), 7.34–7.14 (4H, m, ArH), 6.97 (1H, t, J = 7.6 Hz, ArH), 6.82 (1H, t, J = 7.6 Hz, ArH), 6.43 (1H, t, J = 7.6 Hz, ArH), 5.11 (1H, d, J = 10 Hz, CHCO), 4.57 (1H, t, J = 9.1 Hz, CHPh), 4.14 (1H, q, J = 8 Hz, CHN), 3.72 (1H, d, J = 8.8 Hz), 3.42 (1H, d, J = 8.8 Hz),

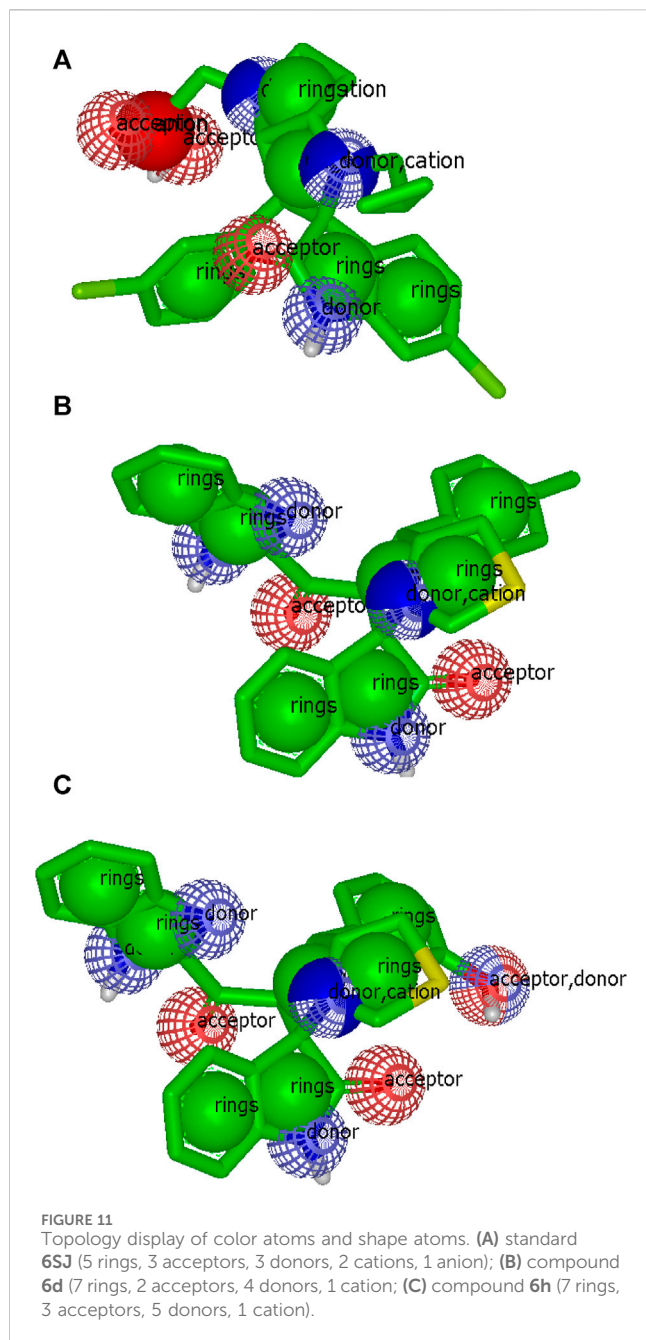
3.09 (1H, dd, J = 11, 5.9 Hz), 2.92 (1H, dd, J = 11, 4.4 Hz); ^{13}C -NMR (101 MHz, DMSO- d_6): δ 189.72, 178.88, 147.75, 143.42, 142.88, 137.30, 134.99, 132.88, 130.31, 129.50, 128.68, 127.37, 126.42, 123.69, 121.85, 121.39, 113.26, 109.96, 75.13, 72.88, 62.72, 52.52, 44.70, 35.44; Anal. for $C_{27}H_{20}Cl_2N_4O_2S$; calcd C, 60.56; H, 3.76; Cl, 13.24; N, 10.46; O, 5.98; S, 5.99; Found: C, 60.50; H, 3.71; Cl, 13.34; N, 10.41; O, 6.03; S, 6.01.

3.1.10 (3*S*,6'*R*)-6'-(1*H*-Benzo [d]imidazole-2-carbonyl)-7'-(3-hydroxyphenyl)-3',6',7',7a'-tetrahydro-1'*H*-spiro [indoline-3.5'-pyrrolo [1,2-*c*]thiazol]-2-one (6h)

White solid; yield (82%); m.p.:205–207°C; IR (KBr, cm^{-1}): 3626 (NH), 3257 (OH), 2931 (CH), 1726 (CO), 1688 (CO); 1H -NMR (400 MHz, DMSO- d_6): δ 12.94 (1H, s, NH), 10.36 (1H, s, NH), 9.46 (1H, s, OH), 7.69 (1H, d, J = 8 Hz, ArH), 7.33 (1H, d, J = 8 Hz, ArH), 7.28 (1H, t, J = 8 Hz, ArH), 7.21 (2H, d, J = 6.7 Hz, ArH), 7.13 (1H, t, J = 8 Hz, ArH), 6.98 (1H, t, J = 7.7 Hz, ArH), 6.89 (2H, d, J = 7.3 Hz, ArH), 6.83 (1H, t, J = 7.3 Hz, ArH), 6.62 (1H, d, J = 8 Hz, ArH), 6.43 (1H, d, J = 8 Hz, ArH), 5.14 (1H, d, J = 11.7 Hz, CHCO), 4.18 (1H, q, J = 8 Hz, CHN), 3.83 (1H, t, J = 10.3 Hz, CHPh), 3.66 (1H, d, J = 8.8 Hz), 3.02 (1H, dd, J = 11.0, 5.9 Hz), 2.92 (1H, dd, J = 10.6, 4.8 Hz); ^{13}C -NMR (101 MHz, DMSO- d_6): δ 190.06, 178.84, 158.20, 147.97, 143.14, 142.94, 141.56, 135.11, 130.12, 127.50, 124.36, 123.55, 121.88, 119.21, 114.98, 109.83, 72.32, 63.26, 51.59, 49.90, 35.27; Anal. for $C_{27}H_{22}N_4O_3S$; calcd C, 67.20; H, 4.60; N, 11.61; O, 9.95; S, 6.64; Found: C, 67.15; H, 4.64; N, 11.65; O, 9.91; S, 6.65.

3.1.11 (3*S*,6'*R*)-6'-(1*H*-Benzo [d]imidazole-2-carbonyl)-7'-(3,4,5-trimethoxyphenyl)-3',6',7',7a'-tetrahydro-1'*H*-spiro [indoline-3.5'-pyrrolo [1,2-*c*]thiazol]-2-one (6i)

White solid; yield (70%); m.p.:245–247°C; IR (KBr, cm^{-1}): 3430 (NH), 3269 (NH), 3093 (CH), 2996 (CH), 1722 (CO), 1683 (CO);



¹H-NMR (400 MHz, DMSO-*d*₆): δ 12.95 (1H, s, NH), 10.35 (1H, s, NH), 7.70 (1H, d, *J* = 8 Hz, ArH), 7.35–7.21 (5H, m, ArH), 7.00 (1H, t, *J* = 7.6 Hz, ArH), 6.85 (2H, d, *J* = 7.7 Hz, ArH), 6.46 (1H, d, *J* = 7.8 Hz, ArH),

5.13 (1H, d, *J* = 11 Hz, CHCO), 4.20 (1H, m, CHN), 3.88 (1H, t, *J* = 9.9 Hz, CHPh), 3.79 (6H, s, OCH₃), 3.69 (1H, d, *J* = 8.8 Hz), 3.60 (3H, s, OCH₃), 3.32 (2H, d, *J* = 3 Hz), 3.03 (2H, m); ¹³C-NMR (101 MHz, DMSO-*d*₆): δ 190.06, 178.90, 153.56, 148.00, 143.13, 142.97, 137.12, 135.94, 135.08, 130.17, 127.79, 126.43, 124.10, 123.64, 121.88, 121.25, 109.89, 105.71, 74.66, 73.00, 62.56, 60.48, 56.47, 52.43, 50.62, 35.70; Anal. for C₃₀H₂₈N₄O₅S; calcd C, 64.73; H, 5.07; N, 10.07; O, 14.37; S, 5.76; Found: C, 64.69; H, 5.10; N, 10.11; O, 14.33; S, 5.77.

3.1.12 (3*S*,6'*R*)-6'-(1*H*-Benzo [d]imidazole-2-carbonyl)-7'-(2-hydroxyphenyl)-3',6',7',7*a*'-tetrahydro-1'*H*-spiro [indoline-3.5'-pyrrolo [1,2-*c*]thiazol]-2-one (6j)

Pale yellow solid; yield (25%); m.p.:186–188°C; IR (KBr, cm⁻¹): 3311 (OH), 3063 (CH), 2925 (CH), 1716 (CO), 1667 (CO); ¹H-NMR (400 MHz, DMSO-*d*₆): δ 12.87 (1H, s, NH), 10.28 (1H, s, NH), 9.63 (1H, s, OH), 7.70 (1H, d, *J* = 8 Hz, ArH), 7.41 (1H, d, *J* = 8 Hz, ArH), 7.34–7.22 (4H, m, ArH), 7.05–6.98 (2H, m, ArH), 6.86–6.76 (3H, m, ArH), 6.44 (1H, d, *J* = 3 Hz, ArH), 5.40 (1H, d, *J* = 11.0 Hz, CHCO), 4.27–4.22 (1H, m, CHN), 3.68 (1H, t, *J* = 9.5 Hz, CHPh), 3.55–3.48 (2H, m), 3.33 (2H, d, *J* = 7.3 Hz); ¹³C-NMR (101 MHz, DMSO-*d*₆): δ 190.40, 178.94, 156.17, 148.15, 143.14, 129.74, 129.31, 129.09, 128.33, 125.87, 124.22, 121.45, 119.85, 115.99, 109.78, 73.56, 73.05, 60.40, 52.69, 44.80, 35.87, 28.42; Anal. for C₂₇H₂₂N₄O₃S; calcd C, 67.20; H, 4.60; N, 11.61; O, 9.95; S, 6.64; Found: C, 67.26; H, 4.66; N, 11.54; O, 9.89; S, 6.65.

3.1.13 (3*S*,6'*R*)-6'-(1*H*-Benzo [d]imidazole-2-carbonyl)-7'-(4-(dimethylamino)phenyl)-3',6',7',7*a*'-tetrahydro-1'*H*-spiro [indoline-3.5'-pyrrolo [1,2-*c*]thiazol]-2-one (6k)

Yellow solid; yield (45%); m.p.:178–180°C; IR (KBr, cm⁻¹): 3434 (NH), 3275 (NH), 3094 (CH), 2929 (CH), 1729 (CO), 1682 (CO); ¹H-NMR (400 MHz, DMSO-*d*₆): δ 12.91 (1H, s, NH), 10.33 (1H, s, NH), 7.69 (1H, d, *J* = 8 Hz, ArH), 7.35–7.21 (6H, m, ArH), 6.99 (1H, t, *J* = 7.7 Hz, ArH), 6.84 (1H, t, *J* = 7.3 Hz, ArH), 6.69 (2H, *J* = 8 Hz, ArH), 6.45 (1H, d, *J* = 8 Hz, ArH), 5.10 (1H, d, *J* = 11.7 Hz, CHCO), 4.20–4.10 (1H, m, CHN), 3.78 (2H, t, *J* = 10.6 Hz, CHPh), 3.67 (2H, d, *J* = 9.5 Hz), 3.54 (3H, d, *J* = 3.7 Hz), 2.95 (2H, m), 2.82 (6H, s, NCH₃); ¹³C-NMR (101 MHz, DMSO-*d*₆): δ 190.23, 178.95, 150.25, 148.05, 143.04, 142.96, 135.07, 130.10, 128.96, 127.69, 127.02, 126.39, 124.37, 123.58, 121.93, 121.34, 113.35, 109.86, 74.50, 72.63, 63.05, 55.45, 52.21, 49.73, 40.70, 35.44; Anal. for C₂₉H₂₇N₅O₂S; calcd C, 68.35; H, 5.34; N, 13.74; O, 6.28; S, 6.29; Found: C, 68.45; H, 5.39; N, 13.54; O, 6.27; S, 6.26.

TABLE 5 Selected physicochemical properties of compounds 6d,h and standard 6Sj as generated by OpenEye software.

Compound	Molecular weight	LogP	PSA	No. of rotatable bond	No. of heavy atom	No. of donor	No. of acceptor
6Sj	488	3.19	75	5	33	4	6
6d	483	2.20	74	3	35	4	6
6h	485	3.19	94	3	35	5	7

3.1.14 (3*S*,6'*R*)-6'-(1*H*-Benzo [d]imidazole-2-carbonyl)-7'-(4-bromophenyl)-3',6',7',7a'-tetrahydro-1'*H*-spiro [indoline-3.5'-pyrrolo [1,2-*c*]thiazol]-2-one (6l)

White solid; yield (80%); m.p.:172–174°C; IR (KBr, cm⁻¹): 3625 (NH), 3422 (NH), 3088 (CH), 2913 (CH), 1725 (CO), 1682 (CO); ¹H-NMR (400 MHz, DMSO-*d*₆): δ 12.95 (1H, s, NH), 10.40 (1H, s, NH), 7.68 (1H, d, *J* = 8 Hz, ArH), 7.55 (2H, d, *J* = 8 Hz, ArH), 7.47 (2H, d, *J* = 8.4 Hz, ArH), 7.36–7.19 (4H, m, ArH), 6.98 (1H, t, *J* = 7.6 Hz, ArH), 6.82 (1H, t, *J* = 7.6 Hz, ArH), 6.43 (1H, d, *J* = 7.6 Hz, ArH), 5.10 (1H, d, *J* = 10.9 Hz, CHCO), 4.24–4.14 (1H, m, CHN), 3.93 (1H, t, *J* = 8 Hz, CHPh), 3.67 (1H, d, *J* = 8.8 Hz), 3.38 (2H, d, *J* = 8.8 Hz), 3.04–2.92 (2H, m); ¹³C-NMR (101 MHz, DMSO-*d*₆): δ 189.88, 178.76, 147.85, 143.23, 142.92, 139.67, 135.10, 132.27, 130.51, 130.10, 127.41, 124.21, 123.99, 121.47, 120.91, 113.25, 109.86, 74.15, 72.34, 62.95, 51.65, 49.41, 33.89; Anal. for C₂₇H₂₁BrN₄O₂S; calcd C, 59.45; H, 3.88; Br, 14.65; N, 10.27; O, 5.87; S, 5.88; Found: C, 59.51; H, 3.81; Br, 14.55; N, 10.31; O, 5.97; S, 5.85.

3.1.15 (3*S*,6'*R*)-6'-(1*H*-Benzo [d]imidazole-2-carbonyl)-7'-(3-fluorophenyl)-3',6',7',7a'-tetrahydro-1'*H*-spiro [indoline-3.5'-pyrrolo [1,2-*c*]thiazol]-2-one (6m)

White solid; yield (30%); m.p.:224–226°C; IR (KBr, cm⁻¹): 3625 (NH), 3422 (NH), 3088 (CH), 2913 (CH), 1725 (CO), 1682 (CO); ¹H-NMR (400 MHz, DMSO-*d*₆): δ 12.97 (s, 1H, NH), 10.41 (s, 1H, NH), 7.68 (d, *J* = 8.1 Hz, 1H, ArH), 7.46–7.19 (m, 7H, ArH), 7.09 (t, *J* = 8.4 Hz, 1H, ArH), 6.98 (t, *J* = 7.7 Hz, 1H, ArH), 6.82 (t, *J* = 7.7 Hz, 1H, ArH), 6.43 (d, *J* = 7.3 Hz, 1H, ArH), 5.11 (d, *J* = 11.0 Hz, 1H, COCH), 4.22 (dt, *J* = 11.0, 5.5 Hz, 1H, CHN), 3.98 (t, *J* = 10.3 Hz, 1H, CHPh), 3.67 (d, *J* = 8.8 Hz, 1H), 3.38 (d, *J* = 5.1 Hz, 1H), 3.04 (dd, *J* = 11.0, 5.9 Hz, 1H), 2.96 (dd, *J* = 11.0, 5.9 Hz, 1H); ¹³C-NMR (101 MHz, DMSO-*d*₆): δ 189.88, 178.79, 147.86, 143.36, 143.23, 142.91, 135.10, 131.42, 131.33, 130.20, 127.44, 126.44, 124.57, 124.17, 123.60, 121.90, 121.38, 115.37, 114.54, 113.27, 109.90, 74.36, 72.39, 63.35, 51.67, 49.41, 35.17; Anal. for C₂₇H₂₁FN₄O₂S; calcd C, 66.93; H, 4.37; F, 3.92; N, 11.56; O, 6.60; S, 6.62; Found: C, 66.84; H, 4.44; F, 3.95; N, 11.49; O, 6.60; S, 6.68.

3.1.16 (3*S*,6'*R*)-6'-(1*H*-Benzo [d]imidazole-2-carbonyl)-7'-(furan-2-yl)-3',6',7',7a'-tetrahydro-1'*H*-spiro [indoline-3.5'-pyrrolo [1,2-*c*]thiazol]-2-one (6n)

White solid; yield (29%); m.p.:240–242°C; IR (KBr, cm⁻¹): 3435 (NH), 3256 (NH), 3090 (CH), 2928 (CH), 1729 (CO), 1687 (CO); ¹H-NMR (DMSO-*d*₆, 400 MHz): δ 13.01 (1H, s, NH), 10.33 (1H, s, NH), 7.71 (1H, d, *J* = 8 Hz, ArH), 7.58 (1H, d, *J* = 4 Hz, ArH), 7.38–7.18 (4H, m, ArH), 6.99 (1H, t, *J* = 7.7 Hz, ArH), 6.83 (1H, t, *J* = 7.7 Hz, ArH), 6.42 (1H, d, *J* = 8 Hz, ArH), 6.40–6.31 (2H, m), 5.14 (1H, d, *J* = 11 Hz, CHCO), 4.20 (1H, m, CHN), 4.02 (1H, t, *J* = 8 Hz, CHPh), 3.66 (1H, d, *J* = 9.5 Hz), 3.37 (2H, d, *J* = 8.8 Hz), 3.12 (2H, m); ¹³C-NMR (DMSO-*d*₆, 100 MHz): δ 189.60, 178.55, 153.16, 147.78, 143.17, 142.99, 135.16, 126.57, 124.00, 110.01, 72.40; Anal. for C₂₅H₂₀N₄O₃S; calcd C, 65.77; H, 4.42; N, 12.27; O, 10.51; S, 7.02; Found: C, 65.73; H, 4.38; N, 12.31; O, 10.47; S, 7.11.

3.1.3 Computational details

“The ωB97X-D (Chai and Head-Gordon, 2008) functional, together with the standard 6–311G (d,p) basis set (Warren et al., 1986) were used in this MEDT study. The TSs were characterized by the presence of only one imaginary frequency. IRC (Fukui, 1970) calculations were performed to establish a unique connection between the TSs and corresponding minima (Gonzalez and Schlegel, 1990; Gonzalez and Schlegel, 1991). Solvent effects of methanol were considered through full optimization of gas phase structures at the same computational level using the polarizable continuum model (PCM) (Tomasi and Persico, 1994; Simkin and Sheikhet, 1995) in the framework of the self-consistent reaction field (SCRf) (Cossi et al., 1996; Cancès et al., 1997; Barone et al., 1998). Values of ωB97X-D/6–311G (d,p) enthalpies, entropies, and Gibbs free energies in methanol were calculated using standard statistical thermodynamics (Warren et al., 1986) at 337.8 K and 1 atm, with PCM frequency calculations at the solvent optimized structures.

The GEDT (Domingo, 2014) values were computed using the equation GEDT(f) = Σq_f, where q represents the natural charges (Reed et al., 1985; Reed et al., 1988) of the atoms belonging to one of the two frameworks (f) in the TS geometries. Global and local CDFT indices were calculated using the equations given in Domingo et al. (2016).

The Gaussian 16 program suite was used to perform the calculations. (Frisch et al. 2016) and ELF (Becke and Edgecombe, 1990) analyses of the ωB97X-D/6–311G (d,p) monodeterminantal wavefunctions were conducted using the TopMod (Noury et al., 1999) package with a cubical grid with a step size of 0.1 Bohr. AIM (Richard et al., 1982) calculations were performed using Multiwfn (Version 3.8) software (Lu and Chen, 2012). Molecular geometries and ELF basin attractors were visualized using GaussView (Serñ and Doğan Ulu, 2023)”.

3.1.4 Molecular docking

The x-ray crystal structure coordinates of the angiotensin receptors were retrieved from PDB (PDB ID: 5law) (Gollner et al., 2016a) with their co-crystallized bound ligand and MDM2. The docking study was performed using OpenEye scientific software, version 2.2.5 (Santa Fe, NM, United States of America) (Gollner et al., 2016a). A virtual library of the synthesized compounds was used; their energies were minimized using the MMFF94 force field, followed by generation of multi-conformers using the OMEGA application. The library was compiled into one file using Omega software. The target proteins were retrieved from PDB, and the created receptor was operated using the OeDocking application. Both ligand and receptor input files were subjected to FRED in the molecular docking study. Multiple scoring functions were used to predict the energy profiles of the ligand–receptor complex. The Vida application was used for visualization. The dimensions for the created box of receptors were as follows. Box volume: 5544 Å, dimensions: 21.00 Å × 18.00 Å × 14.67 Å.

3.1.5 Shape similarity and ROCS analysis

ROCS analysis was performed using OpenEye scientific software. The compound library was used as a database file. Both the query and database files were energy-minimized using Omega applications. The

vROCS was used to run, analyze, and visualize the results. The ROCS application searches the database with a query to identify molecules with similar shapes and colors. The results were visualized using the Vida application. Compound conformers were scored based on the Gaussian overlap with the query. The best scoring parameters were the Tanimoto Combo scores (shape + color); the highest score indicated the best match with the query compound.

4 Conclusion

A new set of spirooxindole hybrids with a benzimidazole unit was designed, synthesized, and further assessed for anti-cancer reactivity. An MEDT study of the 32CA reaction of azomethine ylide (AY) **7a** with ethylene **3a** indicated that the reaction proceeded via a non-concerted *two-stage one-step* mechanism involving a highly asynchronous **TS-on** resulting from the nucleophilic attack of AY **7a** on the β -conjugated position of ethylene **3a**. Formation of two HBs at an earlier stage of the reaction accounted for the *ortho/endo* selectivities experimentally observed in these 32CA reactions. The anti-cancer reactivity results are promising; two compounds (**6a** and **6d**) were identified as most potent, safe, and as p53 activators in triple negative breast (MDA-MB 231) cancer cells to suppress expression, upregulating p21 expression by greater than three times and downregulating the expression of cyclin D and NF- κ B. Moreover, the synthesized compounds showed high binding affinity for MDM2. Compound **6d** showed high similarity in binding mode to the co-crystallized standard ligand. Both compounds showed good physicochemical properties, which motivated us to investigate them further in preclinical studies.

Data availability statement

The original contributions presented in the study are included in the article/[Supplementary Material](#), further inquiries can be directed to the corresponding author.

Author contributions

AB: Conceptualization, Funding acquisition, Supervision, Writing–original draft, Writing–review and editing. SA: Formal Analysis, Investigation, Methodology, Writing–review and editing. AA-M: Supervision, Visualization, Writing–review and editing. AA: Formal Analysis, Investigation, Methodology, Validation, Writing–review and editing. MH: Data curation,

Formal Analysis, Software, Writing–review and editing. MA-S: Data curation, Formal Analysis, Software, Writing–original draft. AD: Formal Analysis, Supervision, Validation, Writing–review and editing. LD: Data curation, Investigation, Software, Validation, Writing–review and editing. YE: Data curation, Software, Validation, Writing–review and editing.

Funding

The author(s) declare financial support was received for the research, authorship, and/or publication of this article. The authors would like to extend their sincere appreciation to the Researchers Supporting Project (RSP2023R64), King Saud University, Riyadh, Saudi Arabia.

Acknowledgments

The authors would like to extend their sincere appreciation to the Researchers Supporting Project (RSP2024R64), King Saud University, Riyadh, Saudi Arabia, project number PID 2019-110776GB-I00 (AEI/FEDER, UE), and Ministerio de Ciencias, Innovación y Universidades of the Spanish Government.

Conflict of interest

The authors declare that the research was conducted in the absence of any commercial or financial relationships that could be construed as a potential conflict of interest.

Publisher's note

All claims expressed in this article are solely those of the authors and do not necessarily represent those of their affiliated organizations, or those of the publisher, the editors and the reviewers. Any product that may be evaluated in this article, or claim that may be made by its manufacturer, is not guaranteed or endorsed by the publisher.

Supplementary material

The Supplementary Material for this article can be found online at: <https://www.frontiersin.org/articles/10.3389/fphar.2024.1358089/full#supplementary-material>

References

- Alshahrani, S., Al-Majid, A. M., Ali, M., Alamy, A. S., Abu-Serie, M. M., Dömling, A., et al. (2023). Rational design, synthesis, separation, and characterization of new spirooxindoles combined with benzimidazole scaffold as an MDM2 inhibitor. *Separations* 10 (4), 225. doi:10.3390/separations10040225
- Amariucai-Mantu, D., Mangalagiu, V., and Mangalagiu, I. (2021). [3 + n] cycloaddition reactions: a milestone approach for elaborating pyridazine of potential interest in medicinal chemistry and optoelectronics. *Molecules* 26, 3359. doi:10.3390/molecules26113359
- Aziz, Y. M. A., Lotfy, G., Said, M. M., El Ashry, E. S. H., El Tamany, E. S. H., Soliman, S. M., et al. (2021). Design, synthesis, chemical and biochemical insights into novel hybrid spirooxindole-based p53-MDM2 inhibitors with potential Bcl2 signaling attenuation. *Front. Chem.* 9, 735236. doi:10.3389/fchem.2021.735236
- Barakat, A., Alshahrani, S., Al-Majid, A. M., Alamy, A. S., Haukka, M., Abu-Serie, M. M., et al. (2022). Novel spirooxindole based benzimidazole scaffold: *in vitro*, nanoformulation and *in vivo* studies on anticancer and antimetastatic activity of

- breast adenocarcinoma. *Bioorg. Chem.* 129, 106124. doi:10.1016/j.bioorg.2022.106124
- Barakat, A., Islam, M. S., Ghawas, H. M., Al-Majid, A. M., El-Senduny, F. F., Badria, F. A., et al. (2019). Design and synthesis of new substituted spirooxindoles as potential inhibitors of the MDM2-p53 interaction. *Bioorg. Chem.* 86, 598–608. doi:10.1016/j.bioorg.2019.01.053
- Barone, V., Cossi, M., and Tomasi, J. (1998). Geometry optimization of molecular structures in solution by the polarizable continuum model. *J. Comput. Chem.* 19, 404–417. doi:10.1002/(sici)1096-987x(199803)19:4<404::aid-jcc3>3.3.co;2-1
- Becke, A. D., and Edgecombe, K. E. (1990). A simple measure of electron localization in atomic and molecular systems. *Chem. Phys.* 92, 5397–5403. doi:10.1063/1.458517
- Beloglazkina, A., Zyk, N., Majouga, A., and Beloglazkina, E. J. M. (2020). Recent small-molecule inhibitors of the p53-MDM2 protein-protein interaction. *Molecules* 25, 1211. doi:10.3390/molecules25051211
- Błaszczak-Świątkiewicz, K. J. M. (2019). Antiproliferative aspect of benzimidazole derivatives' activity and their impact on NF- κ B expression. *Molecules* 24, 3902. doi:10.3390/molecules24213902
- Boggu, P., Venkateswararao, E., Manickam, M., Kim, Y., and Jung, S.-H. J. A. o. p. r. (2017). Exploration of SAR for novel 2-benzylbenzimidazole analogs as inhibitor of transcription factor NF- κ B. *Arch. Pharm. Res.* 40, 469–479. doi:10.1007/s12272-017-0886-1
- Boggu, P., Venkateswararao, E., Manickam, M., Kwak, D., Kim, Y., Jung, S.-H. J. B., et al. (2016). Exploration of 2-benzylbenzimidazole scaffold as novel inhibitor of NF- κ B. *Biorg. Med. Chem.* 24, 1872–1878. doi:10.1016/j.bmc.2016.03.012
- Cancès, E., Mennucci, B., and Tomasi, J. (1997). A new integral equation formalism for the polarizable continuum model: theoretical background and applications to isotropic and anisotropic dielectrics. *J. Chem. Phys.* 107, 3032–3041. doi:10.1063/1.474659
- Chai, J.-D., and Head-Gordon, M. (2008). Long-range corrected hybrid density functionals with damped atom-atom dispersion corrections. *Phys. Chem. Chem. Phys.* 10, 6615–6620. doi:10.1039/b810189b
- Chaudhry, G. E., Md Akim, A., Sung, Y. Y., and Sifzil, T. M. T. (2022). Cancer and apoptosis: the apoptotic activity of plant and marine natural products and their potential as targeted cancer therapeutics. *Front. Pharmacol.* 13, 842376. doi:10.3389/fphar.2022.842376
- Chen, J., Marechal, V., Levine, A. J. J. M., and Biology, c. (1993). Mapping of the p53 and mdm-2 interaction domains. *Mol. Cell. Biol.* 13, 4107–4114. doi:10.1128/mcb.13.7.4107
- Cossi, M., Barone, V., Cammi, R., and Tomasi, J. (1996). *Ab initio* study of solvated molecules: a new implementation of the polarizable continuum model. *Chem. Phys. Lett.* 255, 327–335. doi:10.1016/0009-2614(96)00349-1
- Demma, M., Maxwell, E., Ramos, R., Liang, L., Li, C., Hesk, D., et al. (2010). SCH529074, a small molecule activator of mutant p53, which binds p53 DNA binding domain (DBD), restores growth-suppressive function to mutant p53 and interrupts HDM2-mediated ubiquitination of wild type p53. *J. Biol. Chem.* 285, 10198–10212. doi:10.1074/jbc.M109.083469
- Di Agostino, S., Strano, S., Emiliozzi, V., Zerbini, V., Mottolise, M., Sacchi, A., et al. (2006). Gain of function of mutant p53: the mutant p53/NF-Y protein complex reveals an aberrant transcriptional mechanism of cell cycle regulation. *Cancer Cell* 10, 191–202. doi:10.1016/j.ccr.2006.08.013
- Docking, F. (2016). OpenEye scientific software. Receptor; Version 2.2. 5 Available at: <http://www.eyesopen.com>.
- Domingo, L. R. (2014). A new C-C bond formation model based on the quantum chemical topology of electron density. *RSC Adv.* 4, 32415–32428. doi:10.1039/c4ra04280h
- Domingo, L. R. (2016). Molecular electron density theory: a modern view of reactivity in organic chemistry. *Molecules* 21, 1319. doi:10.3390/molecules21101319
- Domingo, L. R., Pérez, P., and Sáez, J. A. (2013). Understanding the local reactivity in polar organic reactions through electrophilic and nucleophilic Parr functions. *RSC Adv.* 3, 1486–1494. doi:10.1039/c2ra22886f
- Domingo, L. R., Rios-Gutiérrez, M., and Barakat, A. (2022). A molecular electron density theory study of the [3+2] cycloaddition reaction of an azomethine ylide with an electrophilic ethylene linked to triazole and ferrocene units. *Molecules* 27, 6532. doi:10.3390/molecules27196532
- Domingo, L. R., Rios-Gutiérrez, M., and Pérez, P. (2016). Applications of the conceptual density functional theory indices to organic chemistry reactivity. *Molecules* 21, 748. doi:10.3390/molecules21060748
- Domingo, L. R., Rios-Gutiérrez, M., and Perez, P. (2020). A molecular electron density theory study of the participation of tetrazines in aza-Diels-Alder reactions. *RSC Adv.* 10, 15394–15405. doi:10.1039/d0ra01548b
- Domingo, L. R., Saéz, J. A., Zaragoza, R. J., and Arnó, M. (2008). Understanding the participation of quadricyclane as nucleophile in polar [2sigma + 2sigma + 2pi] cycloadditions toward electrophilic pi molecules. *J. Org. Chem.* 73, 8791–8799. doi:10.1021/jo801575g
- Dunphy, G., Flannery, S. M., Almire, J. F., Connolly, D. J., Paulus, C., Jönsson, K. L., et al. (2018). Non-canonical activation of the DNA sensing adaptor STING by ATM and IFI16 mediates NF- κ B signaling after nuclear DNA damage. *Mol. Cell* 71, 745–760. doi:10.1016/j.molcel.2018.07.034
- Estrada-Ortiz, N., Neochoritis, C. G., and Dömling, A. J. C. (2016). How to design a successful p53-MDM2/X interaction inhibitor: a thorough overview based on crystal structures. *Chem. Med. Chem.* 11, 757–772. doi:10.1002/cmdc.201500487
- Frisch, M. J., Trucks, G. W., Schlegel, H. B., Scuseria, G. E., Robb, M. A., Cheeseman, J. R., et al. (2016). *Gaussian 16*. Wallingford, CT: Rev. C.01.
- Fukui, K. (1970). Formulation of the reaction coordinate. *J. Phys. Chem.* 74, 4161–4163. doi:10.1021/j100717a029
- Gollner, A., Rudolph, D., Arnhof, H., Bauer, M., Blake, S. M., Boehmelt, G., et al. (2016a). Discovery of novel spiro [3 H-indole-3,2'-pyrrolidin]-2 (1 H)-one compounds as chemically stable and orally active inhibitors of the MDM2-p53 interaction. *J. Med. Chem.* 59, 10147–10162. doi:10.1021/acs.jmedchem.6b00900
- Gollner, A., Rudolph, D., Arnhof, H., Bauer, M., Blake, S. M., Boehmelt, G., et al. (2016a). Discovery of novel spiro [3H-indole-3,2'-pyrrolidin]-2(1H)-one compounds as chemically stable and orally active inhibitors of the MDM2-p53 interaction. *J. Med. Chem.* 59, 10147–10162. doi:10.1021/acs.jmedchem.6b00900
- Gonzalez, C., and Schlegel, H. (1990). Reaction path following in mass-weighted internal coordinates. *J. Phys. Chem.* 94, 5523–5527. doi:10.1021/j100377a021
- Gonzalez, C., and Schlegel, H. B. (1991). Improved algorithms for reaction path following: higher-order implicit algorithms. *Chem. Phys.* 95, 5853–5860. doi:10.1063/1.461606
- Hsu, Y.-C., and Ip, M. (2011). Conjugated linoleic acid-induced apoptosis in mouse mammary tumor cells is mediated by both G protein coupled receptor-dependent activation of the AMP-activated protein kinase pathway and by oxidative stress. *Cell. Signal.* 23, 2013–2020. doi:10.1016/j.cellsig.2011.07.015
- Islam, M. S., Al-Majid, A. M., Sholkamy, E. N., Barakat, A., Viale, M., Menichini, P., et al. (2023). Optimized spirooxindole-pyrazole hybrids targeting the p53-MDM2 interplay induce apoptosis and synergize with doxorubicin in A549 cells. *Sci. Rep.* 13, 7441. doi:10.1038/s41598-023-31209-3
- Islam, M. S., Ghawas, H. M., El-Senduny, F. F., Al-Majid, A. M., Elshaiher, Y. A., Badria, F. A., et al. (2019). Synthesis of new thiazolo-pyrrolidine-(spirooxindole) tethered to 3-acylindole as anticancer agents. *Bioorg. Chem.* 82, 423–430. doi:10.1016/j.bioorg.2018.10.036
- Janjua, S. (2004). The guardian of genome: p53. *J. Pak. Assoc. Dermatol.* 14, 107–109.
- Jonak, K., Kurpas, M., Szoltysek, K., Janus, P., Abramowicz, A., and Puszynski, K. (2016). A novel mathematical model of ATM/p53/NF- κ B pathways points to the importance of the DDR switch-off mechanisms. *BMC Syst. Biol.* 10, 75. doi:10.1186/s12918-016-0293-0
- Kandath, C., Mclellan, M. D., Vandin, F., Ye, K., Niu, B., Lu, C., et al. (2013). Mutational landscape and significance across 12 major cancer types. *Nature* 502, 333–339. doi:10.1038/nature12634
- Kussie, P. H., Gorina, S., Marechal, V., Elenbaas, B., Moreau, J., Levine, A. J., et al. (1996). Structure of the MDM2 oncoprotein bound to the p53 tumor suppressor transactivation domain. *Science* 274, 948–953. doi:10.1126/science.274.5289.948
- Li, J., Viallet, J., and Haura, E. (2008). A small molecule pan-Bcl-2 family inhibitor, GX15-070, induces apoptosis and enhances cisplatin-induced apoptosis in non-small cell lung cancer cells. *Cancer Chemother. Pharmacol.* 61, 525–534. doi:10.1007/s00280-007-0499-3
- Lotfy, G., Aziz, Y. M. A., Said, M. M., El Sayed, H., El Sayed, H., Abu-Serie, M. M., et al. (2021). Molecular hybridization design and synthesis of novel spirooxindole-based MDM2 inhibitors endowed with BCL2 signaling attenuation; a step towards the next generation p53 activators. *Bioorg. Chem.* 117, 105427. doi:10.1016/j.bioorg.2021.105427
- Lu, T., and Chen, F. (2012). Multiwfn: a multifunctional wavefunction analyzer. *J. Comput. Chem.* 33, 580–592. doi:10.1002/jcc.22885
- Millard, M., Pathania, D., Grande, F., Xu, S., and Neamati, N. J. C. p. d. (2011). Small-molecule inhibitors of p53-MDM2 interaction: the 2006-2010 update. *Curr. Pharm. Des.* 17, 536–559. doi:10.2174/138161211795222649
- Murphy, S. H., Suzuki, K., Downes, M., Welch, G. L., De Jesus, P., Miraglia, L. J., et al. (2011). Tumor suppressor protein (p)53, is a regulator of NF-kappaB repression by the glucocorticoid receptor. *PNAS* 108, 17117–17122. doi:10.1073/pnas.1114420108
- Noury, S., Krokidis, X., Fuster, F., and Silvi, B. J. C. C. (1999). Computational tools for the electron localization function topological analysis. *Comput. Chem.* 23, 597–604. doi:10.1016/s0097-8485(99)00039-x
- Okolotowicz, K. J., Shi, R., Zheng, X., Macdonald, M., Reed, J. C., and Cashman, J. R. (2010). Selective benzimidazole inhibitors of the antigen receptor-mediated NF-kappaB activation pathway. *Bioorg. Med. Chem.* 18, 1918–1924. doi:10.1016/j.bmc.2010.01.039
- Parr, R. (1983). Density functional theory. *Annu. Rev. Phys. Chem.* 34, 631–656. doi:10.1146/annurev.pc.34.100183.003215
- Pires, B. R., Mencialha, A. L., Ferreira, G. M., De Souza, W. F., Morgado-Díaz, J. A., Maia, A. M., et al. (2017). NF-kappaB is involved in the regulation of EMT genes in breast cancer cells. *PLoS One* 12, e0169622. doi:10.1371/journal.pone.0169622
- Poltz, R., and Naumann, M. (2012). Dynamics of p53 and NF- κ B regulation in response to DNA damage and identification of target proteins suitable for therapeutic intervention. *BMC Syst. Biol.* 6, 125. doi:10.1186/1752-0509-6-125

- Reed, A. E., Curtiss, L. A., and Weinhold, F. (1988). Intermolecular interactions from a natural bond orbital, donor-acceptor viewpoint. *Chem. Rev.* 88, 899–926. doi:10.1021/cr00088a005
- Reed, A. E., Weinstock, R. B., and Weinhold, F. (1985). Natural population analysis. *Chem. Phys.* 83, 735–746. doi:10.1063/1.449486
- Richard, F. W., Bader, T.-H. T., Yoram, T., and Friedrich, W. (1982). Properties of atoms and bonds in hydrocarbon molecules. *J. Am. Chem. Soc.* 104, 946–952. doi:10.1021/ja00368a004
- Riedinger, C., and McDonnell, J. (2009). Inhibitors of MDM2 and MDMX: a structural perspective. *Future Med. Chem.* 1, 1075–1094. doi:10.4155/fmc.09.75
- Ríos-Gutiérrez, M., Barakat, A., and Domingo, L. R. (2022). A molecular electron density theory study of the [3+2] cycloaddition reaction of pseudo(mono)radical azomethine ylides with phenyl vinyl sulphone. *Organics* 3, 122–136. doi:10.3390/org3020010
- Serín, S., and Doğan Ulu, Ö. (2023). Theoretical insights into the effects of positional isomerism: DFT/TD-DFT approach. *Avrupa Bilim ve Teknol. Derg.*, 122–135. doi:10.5281/zenodo.10259308
- Siegel, R. L., Miller, K. D., Fuchs, H. E., and Jemal, A. (2021). Cancer statistics, 2021. *CA Cancer J. Clin.* 71, 7–33. doi:10.3322/caac.21654
- Simkin, B. I. A., and Shekhet, I. I. (1995). *Quantum chemical and statistical theory of solutions: a computational approach*. London: Ellis Horwood London.
- Tomasi, J., and Persico, M. (1994). Molecular interactions in solution: an overview of methods based on continuous distributions of the solvent. *Chem. Rev.* 94, 2027–2094. doi:10.1021/cr00031a013
- Tovar, C., Graves, B., Packman, K., Filipovic, Z., Xia, B. H. M., Tardell, C., et al. (2013). MDM2 small-molecule antagonist RG7112 activates p53 signaling and regresses human tumors in preclinical cancer models. *Cancer Res.* 73, 2587–2597. doi:10.1158/0008-5472.CAN-12-2807
- Vassilev, L. (2007). MDM2 inhibitors for cancer therapy. *Trends Mol. Med.* 13, 23–31. doi:10.1016/j.molmed.2006.11.002
- Warren, J., Hehre, L. R., Paul von, R., and Schleyer, J. P. (1986). *AB INITIO molecular orbital theory*, 576. 978-0-471-81241-8.
- Xia, Y., Shen, S., and Verma, I. (2014). NF- κ B, an active player in human cancers. *Cancer Immunol. Res.* 2, 823–830. doi:10.1158/2326-6066.CIR-14-0112
- Zhang, Z., Chu, X.-J., Liu, J.-J., Ding, Q., Zhang, J., Bartkovitz, D., et al. (2014). Discovery of potent and orally active p53-MDM2 inhibitors RO5353 and RO2468 for potential clinical development. *ACS Med. Chem. Lett.* 5, 124–127. doi:10.1021/ml400359z
- Zhao, Y., Liu, L., Sun, W., Lu, J., Mceachern, D., Li, X., et al. (2013). Diastereomeric spirooxindoles as highly potent and efficacious MDM2 inhibitors. *J. Am. Chem. Soc.* 135, 7223–7234. doi:10.1021/ja3125417